Final Report: PARALLELIZED MODELLING AND SOLUTION SCHEME FOR HIERARCHICALLY SCALED SIMULATIONS NAG-31142

Joe Padovan

The University of Akron

Akron, Ohio 44325-3903

Final Report: PARALLELIZED MODELLING AND SOLUTION SCHEME FOR HIERARCHICALLY SCALED SIMULATIONS NAG-31142

Joe Padovan

The University of Akron

Akron, Ohio 44325-3903

Index

Hierarchically Partitioned Solution Strategy For CFD Applications: Part I - Theory

Joe Padovan[Δ]

[Δ]Departments of Mechanical and Polymer Engineering
The University of Akron
Akron, Ohio 44325-3903

Abstract

This two-part paper presents the results of a benchmarked analytical-numerical investigation into the operational characteristics of a unified parallel processing strategy for implicit fluid mechanics formulations. This Hierarchical Poly Tree (HPT) strategy is based on multilevel substructural decomposition. The Tree morphology is chosen to minimize memory, communications and computational effort. The methodology is general enough to apply to existing finite difference (FD), finite element (FEM), finite volume (FV) or spectral element (SE) based computer programs without an extensive rewrite of code. In addition to finding large reductions in memory, communications, and computational effort associated with a parallel computing environment, substantial reductions are generated in the sequential mode of application. Such improvements grow with increasing problem size. Along with a theoretical development of general 2-D and 3-D HPT, several techniques for expanding the problem size that the current generation of computers are capable of solving, are presented and discussed. Among these techniques are several interpolative reduction methods. It was found that by combining several of these techniques that a relatively small interpolative reduction resulted in substantial performance gains. Several other unique features/benefits are discussed in this paper. Along with Part I's theoretical development, Part II presents a numerical approach to the HPT along with four prototype CFD applications. These demonstrate the potential of the HPT strategy.

1 Introduction

The anticipated capacity of supercomputers of the near future falls orders of magnitude short of meeting the demands of Computational Continuum Mechanics (CCM). Weather prediction, combustion modeling, full field aerodynamic simulations, fluid-structure interaction models, among others, are hampered by inadequate computational speed and memory capacity. Limited computer capacities of the past, have fostered the use of explicit methods to maximize the size of the models solved. Their success is due to the facts that they are easy to program, require a minimum of storage, and run fast for simple models that are based on a restrictive set of assumptions. However, as modeling progresses, their weaknesses have surfaced. As the restrictions relax, the resultant set of discretized nonlinear ODEs stiffens. Very small time steps are required for stability. This has sparked a substantial amount of research into the application of implicit methods to Computational Fluid Dynamics (CFD) models [1,2]. Implicit methods require matrix inversion. This inversion can be accomplished in three ways, direct matrix inversion, iteration, or by hybrid methods [3]. Iterative techniques require a minimum of memory. For small matrices, i.e. small models, iterative processes converge quickly, and are faster than direct inversion. However, for the class of CFD problems, large nonlinear sparse, unsymmetric systems, iterative methods are not guaranteed to converge [4]. Furthermore, as the problem size grows, their convergence rate deteriorates to the point that they may become less efficient than direct matrix methods. Iterative methods seem to be popular with researchers, but not with end users who seem are not willing to tolerate the lack of convergence or cannot afford the associated computer costs. In another arena of CCM, Solid Mechanics, the issue of direct matrix inversion versus other inversion techniques, has been settled in the commercial

market place. Virtually all commercially successful, general purpose, solids analysis codes, e.g. NASTRAN, ABAQUS, ADINA, etc., are based on direct matrix inversion (via a variant of Gaussian elimination). In this vein minimization of the effort associated with the direct matrix inversion process is sought.

Previous works by the authors, et.al., have provided lower bound approximations to computational effort and memory requirements associated with the sequential and parallel application of the concept of Hierarchical Poly Trees (HPT) to a broad class of CCM formulations [5-9]. This includes heat transfer and solid mechanics. Linear and nonlinear as well as steady state and transient aspects have been treated. Additionally, the HPT can be employed at the modeling stage, i.e. a preprocessor capable of taking advantage of, and aiding, modeling tasks such as geometric cell cloning, a feature associated mesh enrichment (FAME) [10] etc. Briefly stated, HPT implements multilevel substructural decomposition to achieve reductions in memory, computational effort, and communication requirements. HPT methodology shows increasing computer effectiveness in terms of both memory and computational effort. HPT methodology extends this sequential performance improvement to the parallel processing environment in such a natural way that system overhead is minimized. The HPT methodology is general enough to be applied to existing FD/FV/FEM/SE codes without an extensive rewriting of code and can be implemented on existing parallel computer architectures. Note that the HPT substructural decomposition does not require iteration as do some other domain decomposition techniques such as the subdomain patching methods [11] based on the Schwartz Alternating Scheme (circa 1860's).

In this two-part paper, the authors present the results of research on two and three dimensional fluid formulations employing the Hierarchical Poly Tree (HPT). Along with

a formal analytical-numerical development, the resulting implications in the area of parallel computer processing are presented. This includes the results of several benchmark computational fluid dynamics (CFD) applications.

The main objectives are to i) minimize inversion effort, ii) reduce memory utilization and, iii) limit the communications burden. As will be seen, this can be achieved through the use of the HPT concept. Specifically, what is needed is a reduction in the bandwidths associated with model connectivity. While global minimizers [12] such as those of Cuthill-McKee [13] and Gibbs-Poole-Stockmeyer [14] yield significant improvements, since they are geared primarily to global bandwidth reduction, local characteristics cannot be exploited. As a result, globally minimized models generally consist of thinly populated diagonal and skyline regions. In between these zones is significant numbers of zeros, i.e. Fig. (1). These of course burden the direct inversion process. A remedy to this situation, is to affect the removal of the zeros between the skyline and diagonal matrix regions.

Part I will overview the major features of the HPT as applied and specialized to 2-D and 3-D CFD simulations pertaining to either symmetric or unsymmetric systems of equations. Special emphasis will be given to describe bounds on performance characteristics for simplified geometries. In this context the sections will 1) describe the scheme, ii) develop analytical procedures to optimize the model dependent HPT, and iii) overview potential speedup/memory and communications reductions for simple geometries.

Part II extends the scheme to more general geometries via a numerical scheme. Additionally, comprehensive CFD example problems are presented along with their HPT speedups.

2 The General HPT Methodology

The HPT concept is employed to compress the bandwidth. This is achieved by hierarchically partitioning the model into multilevel substructures. The central focus of the scheme is to eliminate the internal degrees of freedom of each of the various partitions (cells) at every level of the tree. Note, the substructure at the top of the tree generally have narrower bandwidth profiles. This is a direct result of the smallness of the partitions. To maintain the advantage of bandwidth compactness, the partitions chosen at each level must be such that an optimal balance is achieved between the internal and external degrees of freedom. In particular, since the tree requires multiple subassembly steps at each of the various branch levels, the balance between internal and external degrees of freedom must be such that bandwidth compactness is maintained at each and every level. Once this is achieved, a significant number of zeros can be squeezed out of the effort, memory, and communications burden.

There are difficulties associated with the foregoing process. These consist of i) the fact that substructuring intrinsically expands the bandwidth of local partitions, ii) the choice of the proper partition shape is problem dependent and iii) the number of partitions and levels must be determined. The first of these, bandwidth expansion, is a direct outgrowth of the internal-external segregation process central to substructuring, refer to Fig. (2). Recall that the partition level equations take the form

$$[K]\{Y\} = \{F\} \tag{1}$$

The optimal connectivity necessary to minimize the bandwidth of [K] requires an intermixing of internal and boundary nodes. Once substructuring is introduced, (1) is partitioned as follows,

$$\begin{bmatrix} [K_{ii}] & [K_{ie}] \\ [K_{ei}] & [K_{ee}] \end{bmatrix} \begin{bmatrix} \{Y_i\} \\ \{Y_e\} \end{bmatrix} = \begin{bmatrix} \{F_i\} \\ \{F_e\} \end{bmatrix} \tag{2}$$

This process significantly expands the bandwidth, Fig. (2). For example, given an (N,N,N) cubic region, typically the optimal bandwidth is $O(N^2)$. The external-internal partitioning process can expand the mean half bandwidth to $O(6N^2)$ for intermediate level partitions. To overcome the work effort expansion, care must be taken to balance the ratio of internal to external variables in each succeeding branch level. As would be expected, such balancing is intimately tied to the choice of partition shape, the number of branches per level as well as the number of total levels.

2.1 Formulation

For the purpose of developing upper bound analytic estimates of computational effort, memory requirements and communications burden, assume that the cell is a 3-D cube. To balance the tree, decompose the cell into partitions which yield the minimum external/ internal ratios, Fig. (3). This is achieved for cubic zone shapes.

To establish the zone sides and number of levels, the Gaussian elimination process is relied on to determine the operations count. Since the forward matrix reduction phase requires the major effort, it is used to structure the tree architecture. Since cubic regions have an essentially regular node connectivity, the forward effort count (multiply-division-addition pair) takes the form [15]

$$Fe = Ne(BW)^2 \tag{3}$$

such that Ne defines the number of equations and BW is the associated mean half bandwidth. Based on the HPT tree structure the number of branches associated with each succeeding level are given by the tuple

$$K_2,\ K_3,\ldots\ldots,\ K_I.$$

After determining the node connectivity and skyline associated with either a FD grid or finite element model, replace the mean-half-bandwidth with the skyline height in equation (3). The resulting effort for an unsymmetric skylined system can be shown to be the sum of the skyline heights (S_i) squared,

$$Fe = \sum_{i=1}^{n} S_i^2 \tag{4}$$

Memory for the system is then simply the sum of the skyline heights. For discussion purposes the effective mean half bandwidth $(BW)_i$ is determined. To do this, the effects of substructuring induced bandwidth expansion must be taken into account at every branch level.

2.1.1 2-D Formulation

In 2-D the K_i tuple defines k_i dissections per edge of the $(i-1)$th substructure, i.e.,

$$k_i = \sqrt{K_i}\ ;\ i \in [2,\ I] \tag{5}$$

After much symbolic algebra type bookkeeping, it can be shown that, for square zones defined by either 5 noded FD or 4 noded FE models,

$$(BW)_I \approx 3\ \rho\ N_I \tag{6}$$

$$(BW)_i \approx 3.75\ \rho\ N_i;\ i \in [2,\ I-1] \tag{7}$$

$$(BW)_1 \approx 1.75\ \rho\ N \tag{8}$$

where the associated population counts take the form

$$(Ne)_I \approx \rho(N_I)^2 \tag{9}$$

$$(Ne)_i \approx 2\ \rho(k_{i+1}+1)\ N_i;\ i \in [2,\ I-1] \tag{10}$$

$$(Ne)_1 \approx 2\ \rho(k_2 + 1)\ N \tag{11}$$

$$N_i = 1 + (N - 1)/\prod_{l=2}^{i} k_l;\ i \in [2,\ I] \tag{12}$$

such that ρ is the number of degrees of freedom per node and N is the number of nodes per edge. Employing (6-12), the net effort, memory and communications burden can be cast in the following form for sequential type applications.

1) Effort

$$Fe = \sum_{i=1}^{I} (Fe)_i \tag{13}$$

$$(Fe)_I \approx 9\ \rho^3(N_I)^4 \left(\prod_{l=2}^{I} k_l\right)^2 \tag{14}$$

$$(Fe)_i \approx 28.1\ \rho^3(k_{i+1} + 1)\ (N_i)^3 \left(\prod_{l=2}^{i} k_l\right)^2;\ i \in [2,\ I - 1] \tag{15}$$

$$(Fe)_1 \approx 6.12\ \rho^3(k_2 + 1)\ (N)^3 \tag{16}$$

2) Memory

$$Me = \sum_{i=1}^{I} (Me)_i \tag{17}$$

$$(Me)_I \approx 6\ \rho^2(N_I)^3 \tag{18}$$

$$(Me)_i \approx 15\ \rho^2(k_{i+1} + 1)\ (N_i)^2 \left(\prod_{l=2}^{i} k_l\right)^2;\ i \in [2,\ I - 1] \tag{19}$$

$$(Me)_1 \approx 7\ \rho^2(k_2 + 1)\ (N)^2 \tag{20}$$

3) Communications

$$Ce = \sum_{i=2}^{I} (Ce)_i \tag{21}$$

$$(Ce)_i \approx 16\ \rho^2(k_i)^2\ (N_i)^2 \left(\prod_{l=2}^{i} k_l\right)^2;\ i \in [2,\ I] \tag{22}$$

Here *Me* and *Ce* denote the memory and communications burdens. Note the communications requirements are a result of the transfer of the reduced substructural stiffness matrix associated with the external degrees of freedom.

2.1.2 3-D Formulation

In 3-D, the K_i tuple defines k_i dissections per edge of the $(i-1)$th substructure, i.e.,

$$k_i = (K_i)^{1/3};\ i \in [2,\ I] \tag{23}$$

After much bookkeeping and the aid of some symbolic algebra, it can be shown that, for cubic zones of either 7 noded FD or 8 noded FE models,

$$(BW)_I \approx 4\ \rho\ N_I^2 \tag{24}$$

$$(BW)_i \approx 6\ \rho\ N_i^2;\ i \in [2,\ I-1] \tag{25}$$

$$(BW)_1 \approx 3\ \rho\ N^2 \tag{26}$$

where the associated population counts (number of equations) for the HPT take the form

$$(Ne)_I \approx \rho(N_I)^3 \tag{27}$$

$$(Ne)_i \approx 3\ \rho(k_{i+1} + 1)\ N_i^2;\ i \in [2,\ I-1] \tag{28}$$

$$(Ne)_1 \approx 3\ \rho(k_2 + 1)\ N^2 \tag{29}$$

$$N_i = 1 + (N-1)/\prod_{l=2}^{i} k_l;\ i \in [2,\ I] \tag{30}$$

such that ρ is the number of degrees of freedom per node and N is the number of nodes per edge. Employing (24-30), the net effort, memory and communications burden can be cast in the following form for sequential type 3D applications.

1) Effort

$$Fe = \sum_{i=1}^{I} (Fe)_i \tag{31}$$

$$(Fe)_I \approx 16\ \rho^3(N_I)^7 \left(\prod_{l=2}^{I} k_l\right)^3 \tag{32}$$

$$(Fe)_i \approx 108\ \rho^3(k_{i+1} + 1)\ (N_i)^6 \left(\prod_{l=2}^{i} k_l\right)^3;\ i \in [2,\ I - 1] \tag{33}$$

$$(Fe)_1 \approx 27\ \rho^3(k_2 + 1)\ (N)^6 \tag{34}$$

2) Memory

$$Me = \sum_{i=1}^{I} (Me)_i \tag{35}$$

$$(Me)_I \approx 8\ \rho^2(N_I)^5 \left(\prod_{l=2}^{I} k_l\right)^3 \tag{36}$$

$$(Me)_i \approx 36\ \rho^2(k_{i+1} + 1)\ (N_i)^4 \left(\prod_{l=2}^{i} k_l\right)^3;\ i \in [2,\ I - 1] \tag{37}$$

$$(Me)_1 \approx 18\ \rho^2(k_2 + 1)\ (N)^4 \tag{38}$$

3) Communications

$$Ce = \sum_{i=2}^{I} (Ce)_i \tag{39}$$

$$(Ce)_i \approx 36\ \rho^2(N_i)^4 \left(\prod_{l=2}^{i} k_l\right)^3;\ i \in [2,\ I] \tag{40}$$

By proper balancing, *Fe*, *Me*, and *Ce* can be optimized.

2.1.3 Optimization of the HPT Method

Noting the structure of (13-22 and 31-40), it follows that k_i and N_i are nonlinearly coupled throughout the formulation. To obtain an optimal solution, several approaches can be utilized namely, we can minimize *Fe*, *Me* or *Ce* separately or in Lagrange multiplier coupled groups [16]. For the multiplier approach, the criterion function is given by the expression

$$\phi = Fe^* + \mu_1\ Me^* + \mu_2\ Ce^* \tag{41}$$

where effort, memory and communications have been rewritten to conform to the method of Lagrange Multipliers as

$$Fe^*(N_i, k_i) = Fe - \sum_{i=1}^{I} (Fe)_i \tag{42}$$

$$Me^*(N_i, k_i) = Me - \sum_{i=1}^{I} (Me)_i \tag{43}$$

$$Ce^*(N_i, k_i) = Ce - \sum_{i=2}^{I} (Ce)_i \tag{44}$$

Now treating the real world memory limitations and communications burden of a typical computer system as mathematical constraints in the optimization process, we yield the following system.

$$\frac{\partial \phi}{\partial N_i} = 0 \quad i \in [2, I] \tag{45}$$

$$\frac{\partial \phi}{\partial k_i} = 0 \quad i \in [2, I] \tag{46}$$

subject to the constraints

$$Me^* = 0 \quad \text{and} \tag{47}$$

$$Ce^* = 0. \tag{48}$$

Overall (45-48) represent 2I nonlinear equations. Note they provide a linearly weighted optimization of effort, memory and communications burden. Many alternative formulations are possible. To a great extent, the appropriate choice requires specific hardware specifications, i.e. CPU speed, memory capacity, bus transfer speeds, the number of i/o channels, etc.

2.2 Asymptotic Results

For the purpose of obtaining asymptotic expressions for speedup and memory reduction, computational effort will be minimized. This yields the following optimality criteria namely,

$$\frac{\partial Fe}{\partial k_i} = 0;\ i \in [2,\ I] \tag{49}$$

Similar equations apply for the optimization of *Me* or *Ce*.

2.2.1 Asymptotic 2-D Results

Employing (49), the optimal two level tree structure for the square cell is given by the relation

$$k \sim O(N^{1/3}) \tag{50}$$

where here k denotes the number of second (top) level branches for a sequentially processed flow of calculations. The associated speedup relative to the global application of LU decomposition takes the form

$$S \sim O(N^{2/3}) \tag{51}$$

such that S denotes the speedup. For the effort optimized tree, the memory reduction takes the form

$$M_r \sim O(N^{-1/3}) \tag{52}$$

As can be seen from (51 and 52), order of magnitude improvements are afforded by the HPT scheme as the problem size grows. These conveniently apply simultaneously to speedup, memory as well as for communications. Similar but more complex relations can be derived for problems involving several branch levels. The various trends will be discussed later.

2.2.2 Asymptotic 3-D Results

Similarly, the optimal two level tree structure for the cubic cell is given by the relation

$$k \sim O(N^{1/5}) \tag{53}$$

where here k denotes the number of second (top) level branches for a sequentially processed flow of calculations. The associated speedup relative to the global application of LU decomposition takes the form

$$S \sim O(N^{4/5}) \tag{54}$$

such that S denotes the speedup. For the effort optimized tree, the memory reduction takes the form

$$M_r \sim O(N^{-2/5}) \tag{55}$$

2.3 Discussion/Comparison with 2-D Results

The bandwidth associated with the 2-D HPT is of the order O(N); whereas, the bandwidth associated with the 3-D Tree is $O(N^2)$. Thus the later (3-D) is more sensitive to conservative estimates of bandwidth. Since the effort is proportional to the bandwidth squared and memory is proportional to the bandwidth, effort is most affected. Although the analytic expressions have been developed for cubic morphologies, thin 3-D sections can be treated similarly to 2-D for estimations of effort, memory and communications burden, provided that the nodes in the thin direction are accounted for. If the region is somewhat between a thin 3-D shape and a cubic morphology then the speedup and memory reductions will range between those of the 2-D and 3-D HPT. Asymptotic orders of magnitude of improvements associated with 2-D HPTs are well within current computer capacities. But the asymptotic orders of magnitude of 3-D improvements are beyond current computer capacities. In other

words, even though the 3-D HPT has a larger potential for improvement, considering the capacity of current generation computers, exploiting this potential is a challenge. Therefore the next sections present strategies to bring these improvements to current problem size.

2.4 HPT Strategy for Sequential Improvement

As the number of partitions increase, the limiting factor to the increase of speedup and memory reduction is the accumulating root burden. After a point this root burden tends to negate any advantage gained in the upper levels of the tree by increasing the number of partitions. Unfortunately, the root burden dominates early in the 3-D HPT. There are two methods that can eliminate some of the root burden.

- Edge Bisection.
- External Elimination.

These methods will be considered in the following section.

3 Edge-bisection

As pointed out earlier, the accumulation of burden at the root of the Tree, tends to blunt the potential of the 3-D HPT. Earlier work with the 2-D HPT has shown that edge bisection can be effective in the reduction of root burden. This is accomplished as a transfer of some of the root burden to the upper levels of the tree. Edge-bisection means that each successive level in the tree is partitioned in such a way that a 3-D solid would split into eight sections, zones, cells or partitions. That is;

$$k_i = 2;\ i \in [2, I] \tag{56}$$

For example the second level in the 3-D Tree is composed of 8 cells. The third level is composed of 8x8 or 64 cells, and so forth. Refer to Fig. (3) for an illustration of the multilevel Edge-bisection process.

3.1 Formulation

In a manner similar to that of the expressions for the general 3-D case the mean half bandwidth, net effort, memory and communications burden can be cast in the following form for sequential type applications.

$$(BW)_I \approx 4\ \rho[1 + (N - 1)/(2^{I-1})]^2 \tag{57}$$

$$(BW)_i \approx 6\ \rho[1 + (N - 1)/(2^{i-1})]^2;\ i \in [2,\ I - 1] \tag{58}$$

$$(BW)_1 \approx 3\ \rho N^2 \tag{59}$$

where the associated population counts take the form

$$(Ne)_I \approx \rho[1 + (N - 1)/(2^{I-1})]^3 \tag{60}$$

$$(Ne)_i \approx 9\ \rho[1 + (N - 1)/(2^{I-1})]^2;\ i \in [2,\ I - 1] \tag{61}$$

$$(Ne)_1 \approx 9\ \rho N^2 \tag{62}$$

$$N_i = 1 + (N - 1)/\prod_{l=2}^{i} 2;\ i \in [2,\ I] \tag{63}$$

$$N_i = 1 + (N - 1)/(2^{i-1});\ i \in [2,\ I] \tag{64}$$

1) Effort

$$Fe = \sum_{i=1}^{I} (Fe)_i \tag{65}$$

$$(Fe)_I \approx 16\ \rho^3[1 + (N - 1)/(2^{I-1})]^7\ [2^{3(I-1)}] \tag{66}$$

$$(Fe)_i \approx 324\ \rho^3[1 + (N - 1)/(2^{i-1})]^6\ [2^{3(i-1)}];\ i \in [2,\ I - 1] \tag{67}$$

$$(Fe)_1 \approx 81\ \rho^3(N)^6 \tag{68}$$

2) Memory

$$Me = \sum_{i=1}^{I} (Me)_i \tag{69}$$

$$(Me)_I \approx 8\ \rho^2[1 + (N - 1)/(2^{I-1})]^5\ [2^{3(I-1)}] \tag{70}$$

$$(Me)_i \approx 108\ \rho^2[1 + (N - 1)/(2^{i-1})]^4\ [2^{3(i-1)}];\ i \in [2,\ I - 1] \tag{71}$$

$$(Me)_1 \approx 54\ \rho^2(N)^4 \tag{72}$$

3) Communications

$$Ce = \sum_{i=2}^{I} (Ce)_i \tag{73}$$

$$(Ce)_i \approx 288\ \rho^2[1 + (N - 1)/(2^{i-1})]^4\ [2^{3(i-1)}];\ i \in [2,\ I] \tag{74}$$

The Edge-bisection method (EBHPT) yields substantial improvements by increasing the number of levels in the tree rather than increasing the number of partitions; however, the full potential of this method has not yet been fully exploited. The next subsection discusses a process of reducing and/or eliminating external boundary nodes, which in combination with Edge-bisection will provide even greater improvements.

3.2 External-elimination and Edge-bisection

Early removal (at or near the top level) of external boundary nodes from the HPT process can improve performance characteristics. All of these external boundary nodes can be removed at the top level of the tree by any combination of the following two techniques.

- Substructural decomposition/condensation/reduction.
- Assembly.

Treat the external boundary nodes as internals and use substructural decomposition to condense/reduce them from the HPT at the top level. The associated cost is negligible

compared to the overall internal/external reduction process at the top of the tree. Many simulations/models have large portions of their boundaries predetermined (fixed boundary conditions). Fluid simulations are a particular example. In this instance, external boundary nodes are removed at assembly with no appreciable cost to the process. So far the analytic expressions have been based on the effort of interior cells or cells that have not had their externals reduced or eliminated. This leads to over estimation of the effort, memory and communications burden. The Edge-bisected 3-D HPT is particularly sensitive to this, since the root and lower levels are primarily composed of external cells. Modifications to reflect the influence of external cells with their external surface nodes reduced/eliminated, yield expressions for effort, memory and communications burden, where the associated cell population counts take the form.

$$(N_{3S})_i = 1 \tag{75}$$

$$(N_{4S})_i = 3(2^{i-1} - 1) \tag{76}$$

$$(N_{5S})_i = 3(2^{i-1} - 1)^2 \tag{77}$$

$$(N_{6S})_i = (2^{i-1} - 1)^3 \tag{78}$$

These expressions for effort, memory and communications burden are to be found in the Appendix.

3.3 Results of External-elimination and Edge-bisection

The results of the External-elimination and Edge-bisection process are displayed in the graphs that can be found near the end of the next section. The curves ($\gamma = 1.0$) in Figs. (4-8) illustrate the sequential speedup of this process for six level to two level Trees. These figures show that the speedup increases as the size of the problem grows. Two scales are

provided for model size. One of the scales is for total model size (nodes). The other is for nodes/edge. Thus, one can relate the equations (nodes/edge) to total model size. Notice that the speedup for a two level Tree, Fig. (8), saturates with increasing model size. This saturation is easily remedied by increasing the number of levels in the Tree. This can be seen by comparing Fig. (8) to Fig. (7). Also note that increasing the number of levels increases the speedup, provided that the model is large enough. The curves ($\gamma = 1.0$) in Figs. (9-13) illustrate the memory reduction associated with the External-elimination and Edge-bisection process for six level to two level Trees. These figures show trends similar to the speedup trends. Although substantial improvements are shown in these graphs, the desire to extend the capabilities of the current generation computers to even larger problems leads to further strategies for improvement.

3.4 Further Strategies for Improvement

While the previous specializations of the HPT have lead to performance gains, the following methods can lead to further improvements in performance;

- Interpolative Reduction.
- Hybrid Methods.
- Parallelism.

Before parallelism is discussed, the other sequential improvement strategies will be exploited in the next sections, so that parallelism can further enhance these sequential gains.

4 Interpolative Reduction Methodology

The concept of interpolative reduction is to add or provide local information, i.e. stress concentration, turbulence, etc., in a way that is more economical than grid/mesh refinement.

Interpolative reduction by levels adds a scaling capability to the HPT, that could be used to simulate a physical process involving scales [17]. The following methods of interpolative reduction are discussed.

- Throw-Away Method.
- Substructural Reduction.
- Interpolation.

The throw-away or matrix stripping method is the crudest form of interpolation possible. In this method, the row and column of the node to be reduced is stripped from the matrix of externals before passing the matrix to the next level. This process essentially results in decoupling the equations involving the reduced node from the rest of the system. Since this is a zero interpolation process, i.e. no information is transferred to any of the surrounding nodes, this is the cheapest form of interpolative reduction. The substructural reduction method consists of treating the node to be reduced as an internal node during the substructural decomposition process, in order to affect interpolative reduction. The following two constraint methods are used to enforce a nonzero interpolation reduction.

- Energy Method
- Least Squares

After considering the constraint methods of the interpolative reduction process, some consideration must be given as to how this process can be most effectively incorporated within the HPT process. The interpolative reduction process can be employed at two stages in the Tree process.

- After Assembly.
- Before Assembly.

Note that the HPT method bears no similarities to multigrid iterative schemes, where the results of a coarse grid/mesh are interpolated as an initial guess (preconditioner) to a finer grid for the purpose of accelerating convergence.

The next subsections discuss the constraint processes and their implementation before and after assembly.

4.1 Energy Method for Symmetric, Positive Definite Systems

The energy method results in an efficient interpolation, where the energies in both the original system and the interpolated system have the same average energy. The interpolation process for symmetric, positive definite systems begins by considering the stiffness equation resulting from the discretization process.

$$[K]\ \{Y\} = \{F\} \tag{79}$$

Then this can be formed into a force residual equation as,

$$\{r\} = [K]\ \{Y\} - \{F\} \tag{80}$$

From work concepts $(\overline{F} \cdot d\overline{r})$, multiply by $\{Y\}^T$.

$$\{Y\}^T\ \{r\} = \{Y\}^T\ [K]\ \{Y\} - \{Y\}^T\ \{F\} \tag{81}$$

Thus define an energy residual.

$$\{r\}_e = \frac{1}{2}\ \{Y\}^T\ [K]\ \{Y\} - \{Y\}^T\ \{F\} \tag{82}$$

Given the interpolation constraint/curve fit,

$$\{Y\} = [T]\ \{\hat{Y}\}, \tag{83}$$

its application to the energy residual yields

$$\{r\}_e = \frac{1}{2}\ \{\hat{Y}\}^T\ [T]^T\ [K]\ [T]\ \{\hat{Y}\} - \{\hat{Y}\}^T\ [T]^T\ \{F\} \tag{84}$$

Minimizing the energy residual gives

$$\frac{\partial}{\partial \hat{Y}_i} \{r\}_e = [T]^T [K] [T] \{\hat{Y}\} - [T]^T \{F\} = 0 \tag{85}$$

Now then the energy interpolation transform is defined.

$$[\hat{K}] \{\hat{Y}\} = \{\hat{F}\} \tag{86}$$

$$[\hat{K}] = [T]^T [K] [T] \tag{87}$$

$$\{\hat{F}\} = [T]^T \{F\} \tag{88}$$

However, [K] can be nonsymmetric, nonpositive definite, i.e. for general fluid simulations. This method of minimizing the energy residual to define the interpolative reduction is not applicable in this situation. Thus, a least squares minimization technique is employed to prescribe the interpolative reduction process.

4.2 LS Method for Nonsymmetric/Nonpositive Definite Systems

The least squares method results in an interpolation, where the least squares residual is minimized between the original system and the interpolated system [18-20]. The interpolation process for unsymmetric nonpositive definite systems begins by considering the stiffness equation resulting from the discretization process. The top level stiffness matrix created by the FD/FV/FEM/SPE discretization process, (79), can be cast in a residual form, namely (80). Applying the interpolative reduction (constraint/curve fit) given by (83), the stiffness matrix formulation and the residual equation yields,

$$[K] [T] \{\hat{Y}\} = \{F\} \tag{89}$$

$$\{r\} = [K] [T] \{\hat{Y}\} - \{F\} \tag{90}$$

Now apply the least squares method to the above equations by squaring the residual

$$\{r\}^T \{r\} = ([K] [T] \{\hat{Y}\} - \{F\})^T ([K] [T] \{\hat{Y}\} - \{F\}) \tag{91}$$

and minimizing wrt. to $\{\hat{Y}\}$,

$$\frac{\partial}{\partial \hat{Y}_i} \{r\}^T \{r\} = 0 \tag{92}$$

yields,

$$[K]^T [T]^T ([K] [T] \{\hat{Y}\} - \{F\}) = 0 \tag{93}$$

Now writing the interpolatively reduced system of equations as,

$$[\hat{K}] \{\hat{Y}\} = \{\hat{F}\} \tag{94}$$

Comparing equations defines the interpolated stiffness matrix $[\hat{K}]$ and the interpolated force vector $\{\hat{F}\}$ as

$$[\hat{K}] = [T]^T [K]^T [K] [T] \tag{95}$$

$$\{\hat{F}\} = [T]^T [K]^T \{F\} \tag{96}$$

Notice that the interpolated stiffness matrix is symmetric and positive definite.

4.3 Interpolation After Substructural Decomposition

Interpolative reduction after substructural decomposition (IRA) process reduces/interpolates the resultant condensed stiffness matrix, which is composed of the external nodes of the internal/external segregation process. Then the reduced matrix of externals is transferred to next level in a downward progression. This reduction process relieves the congestion occurring at the lower levels. Then starting at the top of the Tree, the next expression defines the number of nodes at the top of an Ith level Tree.

$$N_I = 1 + (N - 1)/(2^{I-1}) \tag{97}$$

For interpolative reduction after substructural decomposition the number of nodes at the current level are reduced from the number of nodes at the previous level by the relation.

$$N_i = 1 + 2(\gamma_{i+1} N_{i+1} - 1);\ i \in [1, I - 1] \tag{98}$$

where γ_i is the nodes/edge reduction ratio. With the population count defined (97, 98), the relations given in the appendix (A1-A29) for effort memory and communications are employed to describe the results of the interpolative reduction after substructural decomposition (IRA) process.

Of course the interpolation could be applied elsewhere in the HPT. Another possibility would be to consider an interpolative reduction applied before the substructural decomposition (IRB) process, i.e. directly after assembly. This would allow one more reduction in the Tree to take place; and, the effort and memory associated with substructural decomposition phase would be reduced. It was found that the interpolation costs of this method overwhelmed the aforementioned benefits. Thus, the IRB method will not be discussed further.

The next subsection presents the results of the interpolative reduction after substructural decomposition (IRA) process.

4.4 Results of Interpolative Reduction

The results of interpolative reduction after substructural decomposition (IRA) process are displayed graphically in Figs. (4-13) for Edge Bisected, Externals Eliminated, Trees. The effort associated with various level Trees (6th level to 2nd level) is shown in Figs. (4-8) and memory in Figs. (9-13). These figures show increases in performance associated with the following trends:

- increasing the number of levels in the Tree.
- increasing model size.
- increasing interpolative reduction (decreasing γ).

The curves in the graphs correspond to equipresent reduction ratios. An equipresent reduction ratio refers to applying the same reduction ratio to all levels of the Tree. The ratios used are:

- $\gamma = 1.0$ (no reduction),
- $\gamma = 0.9$ (0.729 global reduction ratio per level),
- $\gamma = 0.8$ (0.512 global reduction ratio per level),
- $\gamma = 0.7$ (0.343 global reduction ratio per level).

The effect of symmetrization can be seen in the jump from the $\gamma = 1.0$ (no reduction) curve to the $\gamma = 0.9$ curve in each of the figures. Symmetrization is the primary cause of this jump and the reduction is a minor effect. The jumps between the other curves, excluding $\gamma = 1.0$, show the interpolative reduction effects. As the number of levels increases the curves begin at larger model sizes. This reflects that the higher level Trees require larger models. The figures show that the two level Tree is the only tree that cannot pay for the cost of interpolative reduction, see Figs. (8 and 3).

The range of model sizes covers current and future sized models, where a 100x100x100 3-D model (1 million) equations is considered the practical upper limit of current computers. The range of the next generation of models is considered to be a decade increase in resolution in each dimension, or a 100x100x100 3D model (1 million) equations as a lower bound and a 1000x1000x1000 3-D model (1 Billion) equations as the upper limit of the next generation of models. In this context the 3-D HPT is showing substantial improvements for current and next generation models with and without interpolative reduction. These figures fairly well summarize the sequential 3-D HPT process as presented.

5 Hybrid Methods

Before considering the performance gains available from parallel processing, several significant remaining aspects of improving sequential processing will be discussed. These are grouped and classified under the title of hybrid methods.

- Iterative/Direct solve at Root.
- Symmetric/Unsymmetric Formulations.

The first of these hybrid methods considered is that of combining iterative solvers with the HPT. For certain simulations global iterative solvers can be more effective than global direct solvers. But again, this is highly problem dependent. In these situations the root burden can be reduced by an efficient iterative solver of the following types:

- steepest descent.
- preconditioned conjugate gradient.

The effort improvement depends on the rate of convergence which, in turn, is dependent on the particular implementation of the iterative solver, the initial guess used to start the solver, the particular simulation, and ratio of the root burden to the overall computational burden. Previously it has been demonstrated that even through the use of multilevel edge bisection, which has been employed to reduce the root burden, the root is the single largest HPT burden. The memory (number of memory locations) for the iterative solver is now equivalent to the number of equations (Ne), assuming that the iterative solver requires auxiliary storage much less than O(Ne). This represents two orders of magnitude of improvement in the root memory requirements. Thus, the iterative/direct hybrid HPT is an effective strategy, when applicable. The applicability can be determined on the fly, by monitoring the rate of convergence, comparing the accumulating solve effort to estimated

direct solve effort. If the rate of convergence deteriorates or the solve effort exceeds that of the direct solver, the program can then switch to the direct solver. The beforehand checks that could be employed are the matrix condition number of the system. Certain formulations of certain simulations are known, apriori, to have poor condition numbers for convergence. Matrix density is another parameter that can be tested. Iterative techniques are not generally used to invert full matrices, because there is no savings in storage, the effort savings due to sparsity has disappeared, and they do not generally have good convergence properties.

The second hybrid method considered is that of the symmetric/unsymmetric HPT. There are two considerations. First, the least squares interpolation method has been shown to symmetrize the system matrix resulting from discretization processes. If this symmetrization is taken advantage of at the top of the tree then memory reduction and speedup gains occur at each and every successive level in the tree, by halving the computational effort and memory requirements. The second consideration of the symmetric/ unsymmetric hybrid HPT is the consideration of regions that may be either a symmetric or unsymmetric formulation within the same simulation, e.g. fluid-structure interaction simulations. Thus, the HPT has capability to regularize a model, in terms of merging a symmetric/unsymmetric problem into a symmetric one.

6 Parallelization of HPT

In parallel computing environments, the tree structure can be used to establish the flow of control, communications and problem assembly. Overall, several types of parallel architecture can be defined for the foregoing HPT formulation. These include:

1. Fully parallelized, wherein each partition of the tree is provided its own processor with either shared or local memory.
2. Partially parallelized, wherein P singly assigned processors are leapfrogged from substructure to substructure level by level, see Fig. (14), or
3. Partially parallelized, wherein a total of P processors are organized into G groups which are separately leapfrogged to various partitions, level by level, such that several processors may be assigned to a given partition, Fig. (15).

Note for case 3) involving multiple assignment, since such architectures tend to reach saturation when too many processors are locally involved, the choice of P and G is machine dependent. Here of course the main goal is to maximize the superlinearity. A further aspect of cases ii) and iii) follows from the fact that as the forward elimination process moves down the tree, the number of processors may become greater than that of the branches. For such situations, the multiple assignment factor P/G may be raised to improve utility; if saturation is not reached.

Based on the prior comments on parallelism, the expression defining Fe needs to be altered. In particular, modifications must be introduced to account for such features as full/partial parallelism, single/multiple assignment and, single/multi processor efficiency. This process leads to the following formulations:

i) 2-D fully parallel

$$P_f\{Fe\} \approx 6.12\ \rho^3(k_2 + 1)\ N^3 + \left[\sum_{i=2}^{I-1} 28.1\ \rho^3(k_{i+1} + 1)\ (N_i)^3\right] + 9\ \rho^3(N_I)^4 \quad (99)$$

ii) 2-D partially parallel-single/multi assignment

$$P_p\{Fe\} = \sum_{i=1}^{I} (Fe)_{pi} \quad (100)$$

$$\{Fe\}_{pI} \approx \frac{9\ \rho^3(N_I)^4}{E\ P}\left(\prod_{l=2}^{I} k_l\right)^2 \tag{101}$$

$$\{Fe\}_{pi} \approx \frac{28.1\ \rho^3(k_{i+1}+1)\ (N_i)^3}{E\ P}\left(\prod_{l=2}^{i} k_l\right)^2;\ i \in [2,\ I-1] \tag{102}$$

$$\{Fe\}_{p1} \approx 6.12\ \rho^3(k_2+1)\ (N)^3/(E\ P) \tag{103}$$

iii) 3-D fully parallel,

$$P_f\{Fe\} \approx 27\ \rho^3(k_2+1)\ N^6 + \left[\sum_{i=2}^{I-1} 108\ \rho^3(k_{i+1}+1)\ (N_i)^6\right] + 16\ \rho^3(N_I)^7 \tag{104}$$

iv) 3-D partially parallel-single/multi assignment

$$P_p\{Fe\} = \sum_{i=1}^{I} (Fe)_{pi} \tag{105}$$

$$\{Fe\}_{pI} \approx \frac{16\ \rho^3(N_I)^7}{E\ P}\left(\prod_{l=2}^{I} k_l\right)^3 \tag{106}$$

$$\{Fe\}_{pi} \approx \frac{108\ \rho^3(k_{i+1}+1)\ (N_i)^6}{E\ P}\left(\prod_{l=2}^{i} k_l\right)^3;\ i \in [2,\ I-1] \tag{107}$$

$$\{Fe\}_{p1} \approx 27\ \rho^3(k_2+1)\ (N)^6/(E\ P) \tag{108}$$

such that E denotes machinery efficiency. Noting case ii), the speedup potential afforded by employing the HPT framework to parallelize calculations can be very significant. For example considering the two level tree, then for 2-D simulations,

$$P_p\{S\} \sim O(N^{2/3})\ E\ P \tag{109}$$

and for 3-D simulations,

$$P_p\{S\} \sim O(N^{4/5})\ E\ P \tag{110}$$

Depending on problem size, even better optimalities are afforded by introducing multiple branch levels. The partially parallelized HPT yields the following effort requirement namely

$$P_p\{Fe(net)\} = \frac{1}{P}\{Fe(root) + N_c\ Fe(unit\ cell)\} \tag{111}$$

Equation (111) can be interpreted in two ways. In particular, the unit cells can be handled via either single or multiple assignment leapfrogging. For the single case, only one processor is scheduled to handle a given partition's operational needs. These requirements change depending on whether the forward elimination or back substitution phases of computation are involved. Note that the forward phase involves a downward flow of control in the tree. In contrast, back substitution requires an upward flow of control. For the multiple assignment architecture, the various operational steps are shared among the various processors scheduled for the given substructure. If multi-assignment processor saturation is taken into account, then (111) reduces to the form

$$P_{ps}\{Fe(net)\} = \frac{1}{E\ P_s}\{Fe(root) + N_c\ Fe(unit\ cell)\} \tag{112}$$

where P_s denotes the allowable upper bound on the number of processors that can be dedicated to a given programming task. In the case where $P_s < P$ is satisfied at all the various branch levels, then (111) reverts to (112).

7 Discussion and Conclusions

This paper has presented the results of an analytic investigation into the characteristics of a unified parallel processing strategy for implicit, three dimensional formulations. For 2-D and 3-D FD/FV/FEM/SE models, the HPT offers very attractive asymptotic computational speedups, memory reductions and minimized communications. In a coarse-grained parallel computing environment, where processor leapfrogging is employed to handle the tree, the effort reduction is proportional to $E\ P$, namely for 2-D models

$$P\{S\} \sim O(N^{2/3})\ E\ P \tag{113}$$

and for 3-D models

$$P\{S\} \sim O\{(\text{Problem Size})^{4/5}\}\ E\ P \tag{114}$$

Note since the Tree provides for individual updating of each of the top level branches, the model stiffness regeneration effort is reduced by the same factor ($E\ P$). Overall, the HPT forms a naturally parallelizable communications link. Since it minimizes memory and effort, hardware demands are also reduced. This is not the case with recent attempts at parallelizing direct global solvers, which leave the memory and effort requirements unchanged. In addition to finding large reductions in memory, communications, and computational effort associated with a parallel computing environment, substantial reductions have been generated in the sequential mode of application. Such improvements grow with increasing problem size. In the case of models with relatively cubic morphologies, as problem size becomes very large, the following asymptotic, many orders of magnitude, effort and memory reductions occur for sequential computer environments, namely for 2-D simulations,

$$S \sim O\{(\text{Problem Size})^{2/3}\} \tag{115}$$

$$M_r \sim O\{(\text{Problem Size})^{1/3}\} \tag{116}$$

and for 3-D simulations,

$$S \sim O\{(\text{Problem Size})^{4/5}\} \tag{117}$$

$$M_r \sim O\{(\text{Problem Size})^{2/5}\} \tag{118}$$

Similar trends apply for the communications requirements. Optimality considerations were given to these performance factors, showing i.) how the 3-D Tree can be tuned for peak performance, and ii.) some results of this tuning process.

In addition to a theoretical development of the general 3-D HPT methodology, several techniques, for expanding the problem size that the current generation of computers are capable of solving, have been presented and discussed. Among these techniques that have

been discussed, are several interpolative reduction methods. Some of these techniques have 2-D applications as well. It was found that by combining several of these techniques that a relatively small interpolative reduction resulted in substantial performance gains. Possibly the most significant finding was that previously prohibitively computationally expensive procedures can be employed at the top level of a multi-level tree without significantly affecting memory, communications and computational effort. For example, least squares formulations are particularly effective when the system of governing equations are cast in a first order form. This removes two major difficulties. First the inter-element continuity requirements are lowered. And second, the problems associated with terms of different order, e.g. the pressure and velocity terms in an incompressible flow simulation or in the case of modeling of incompressible materials, disappears. These gains are obtained at the cost of increasing the size of the system of equations that must be solved. Due to the already overburdened and limited capacity of current generation computers, the potential of least squares and other computationally expensive formulations have not been exploited on a large scale. However, when employed at the top level of a hybrid multi-level Tree these previously prohibitively computationally expensive procedures become very cost effective.

It should be pointed out that, it is expected that in practice one will find the speedups and memory reductions to be larger than those projected in this paper for two main reasons:

- The assumptions that the analytic expressions have been based on, are conservative; and in practice,
- the system matrix of each partition on each level can be optimized before substructural condensation or solution.

Numerical studies and applications of the HPT have verified the assertion that the analytic expressions are conservative for both sequential and parallel computations for the 2-D Tree. It is hoped that the results of this work will be useful in the design and implementation of the next generation of computing hardware.

References - Part One

[1] A.J. Baker, Finite Element Computational Fluid Mechanics, McGraw-Hill, N.Y., 1983.

[2] Thomas H. Pulliam, Implicit Methods in CFD, Eds. K.W. Morton and M.J. Baines, Numerical Methods for Fluid Dynamics and Aerodynamics III, Clarendon Press, 1988.

[3] K. Gallivan, A. Sameh and Z. Zlative, A Parallel Hybrid Sparse Linear Systems Solver, Computing Systems in Engineering, Vol. 1, Nos. 2-4, pp. 183, 195, 1990.

[4] C. Cuvelier, A. Segal and A.A. Von Steenhoven, F.E.M. and N-S Equations, D. Reidel, Boston, 1986.

[5] J. Padovan, Nonlinear Hierarchical Substructural Parallelism and Computer Architecture, Computational Mechanics CSM Workshop presented at NASA-Langley, June 1985.

[6] J. Padovan, D. Gute, and K. Johnson, Hierarchical Poly Tree Computer Architectures Defined by Computational Multidisciplinary Mechanics, Computers and Structures, Vol. 32, No. 5, pp. 1133-1163, 1989.

[7] D. Gute, Hierarchical Poly Tree Computer Architectures for the Solution of Finite Element Formulations, Ph.D. Dissertation, University of Akron, January 1990.

[8] J. Padovan and A. Kwang, Hierarchically Parallelized Constrained Nonlinear Solvers with Automated Substructuring, Vol. 41, No. 1, pp. 7-33, 1991.

[9] J. Parris, Hierarchical Poly Tree Methodology and Partitioned Implicit Fluid Simulations, Ph.D. Dissertation, University of Akron, May 1992.

[10] C.M. Albone, An Approach to Geometric and Flow Complexity Using Feature-Associated Mesh Embedding (FAME): Strategy and First Results, Eds. K.W. Morton and M.J. Baines, Numerical Methods for Fluid Dynamics and Aerodynamics III, Clarendon Press, pp. 215-235, 1988.

[11] X. Cai and O. Widlund, Domain Decomposition Algorithms for Indefine Elliptic Problems, Siam J. Sci. Stat. Comput., Vol. 13, pp. 243-258, 1992.

[12] A. George and J. Liu, Computer Solution of Large Sparse Positive Definite Systems, Prentice-Hall, Englewood Cliffs, N.J., 1981.

[13] E. Cuthill and J. McKee, Reducing the Bandwidth of Sparse Symmetric Matrices, Proc. ACM National Conference, pp. 157-172, 1969.

[14] N.E. Gibbs, W.G. Poole, and P.K. Stockmeyer, An Algorithm for Reducing the Bandwidth and Profile of a Sparse Matrix, SIAM Journal of Numerical Analysis, Vol. 13, pp. 236-250, 1976.

[15] K.J. Bathe, Finite Element Procedures in Engineering Analysis, Prentice-Hall, Englewood Cliffs, N.J., 1982.

[16] M.M. Denn, Optimization by Variational Methods, McGraw-Hill, N.Y., 1969.

[17] A.J. Reynolds, Turbulent Flows in Engineering, Wiley, N.Y., 1974.

[18] P.P. Lynn and S.K. Arya, Use of the Least Squares Criterion in the Finite Element Formulation, International Journal for Numerical Methods in Engineering, Vol. 6, pp. 75-88, 1973.

[19] C.A.J. Fletcher, A Primative Variable Finite Element Formulation for Inviscid, Compressible Flow; Journal of Computational Physics, Vol. 33, pp. 301-312, 1979.

[20] B.N. Jiang and G.F. Carey, Adaptive Refinement for Least-Squares Finite Elements with Element-by-Element Conjugate Gradient Solution, International Journal for Numerical Methods in Engineering, Vol. 24, pp. 569-580, 1987.

Appendix

HPT Effort Memory and Communications Burden associated with external-elimination and edge-bisection.

1) Effort

$$Fe = \sum_{i=1}^{t} (Fe)_i \tag{A1}$$

$$(Fe)_i = 8\,[(N_{3S})_i\,(Fe_{3S})_i + (N_{4S})_i\,(Fe_{4S})_i + (N_{5S})_i\,(Fe_{5S})_i + (N_{6S})_i\,(Fe_{6S})_i] \tag{A2}$$

$$(Fe_{3S})_I \approx \frac{1}{4}\rho^3[25N_I^7 - 105N_I^6 + 184N_I^5 - 178N_I^4 + 106N_I^3 - 40N_I^2 + 9N_I - 1] \tag{A3}$$

$$(Fe_{4S})_I \approx \frac{1}{4}\rho^3[36N_I^7 - 204N_I^6 + 469N_I^5 - 588N_I^4 + 449N_I^3 - 214N_I^2 + 60N_I - 8] \tag{A4}$$

$$(Fe_{5S})_I \approx \frac{1}{4}\rho^3[49N_I^7 - 357N_I^6 + 1{,}072N_I^5 - 1{,}756N_I^4 + 1{,}744N_I^3 - 1{,}072N_I^2 + 384N_I - 64] \tag{A5}$$

$$(Fe_{6S})_I \approx 4\rho^3[4N_I^7 - 36N_I^6 + 137N_I^5 - 290N_I^4 + 376N_I^3 - 304N_I^2 + 144N_I - 32] \tag{A6}$$

$$(Fe_{3S})_i \approx \frac{1}{48}\rho^3[2{,}230N_i^6 - 25{,}705N_i^5 + 125{,}225N_i^4 - 329{,}654N_i^3 + 494{,}316N_i^2 - 400{,}257N_i + 136{,}725] \tag{A7}$$

$$(Fe_{4S})_i \approx \frac{1}{48}\rho^3[3{,}737N_i^6 - 41{,}998N_i^5 + 200{,}645N_i^4 - 518{,}746N_i^3 + 761{,}837N_i^2 - 599{,}776N_i + 197{,}181] \tag{A8}$$

$$(Fe_{5S})_i \approx \frac{1}{48}\rho^3[5{,}865N_i^6 - 56{,}029N_i^5 + 231{,}218N_i^4 - 525{,}254N_i^3 + 691{,}273N_i^2 - 499{,}461N_i + 155{,}28] \tag{A9}$$

$$(Fe_{6S})_i \approx \frac{1}{48}\rho^3[8{,}977N_i^6 - 56{,}596N_i^5 + 244{,}730N_i^4 - 560{,}564N_i^3 + 718{,}197N_i^2 - 505{,}104N_i + 156{,}024] \quad \text{(A10)}$$

$$i \in [2, I-1]$$

$$(Fe)_1 \approx \frac{1}{48}\rho^3[217N_i^6 - 3{,}157N_i^5 + 19{,}148N_i^4 - 62{,}054N_i^3 + 113{,}481N_i^2 - 111{,}189N_i + 45{,}666] \quad \text{(A11)}$$

2) Memory

$$Me = \sum_{i=1}^{I} (Me)_i \quad \text{(A12)}$$

$$(Me)_i = 8\,[(N_{3S})_i\,(Me_{3S})_i + (N_{4S})_i\,(Me_{4S})_i + (N_{5S})_i\,(Me_{5S})_i + (N_{6S})_i\,(Me_{6S})_i] \quad \text{(A13)}$$

$$(Me_{3S})_I \approx \rho^2[5N_I^5 - 11N_I^4 + 8N_I^3 - 6N_I^2 + 3N_I - 1] \quad \text{(A14)}$$

$$(Me_{4S})_I \approx \rho^2[6N_I^5 - 15N_I^4 + 13N_I^3 - 9N_I^2 + 5N_I - 2] \quad \text{(A15)}$$

$$(Me_{5S})_I \approx \rho^2[7N_I^5 - 20N_I^4 + 21N_I^3 - 14N_I^2 + 8N_I - 4] \quad \text{(A16)}$$

$$(Me_{6S})_I \approx \rho^2[8N_I^5 - 26N_I^4 + 33N_I^3 - 23N_I^2 + 12N_I - 8] \quad \text{(A17)}$$

$$(Me_{3S})_i \approx \frac{1}{2}\rho^2[58N_i^4 - 450N_i^3 + 1{,}341N_i^2 - 1{,}816N_i + 943] \quad \text{(A18)}$$

$$(Me_{4S})_i \approx \frac{1}{4}\rho^2[162N_i^4 - 1{,}205N_i^3 + 3{,}451N_i^2 - 4{,}491N_i + 2{,}235] \quad \text{(A19)}$$

$$(Me_{5S})_i \approx \frac{1}{4}\rho^2[217N_i^4 - 1{,}400N_i^3 + 3{,}586N_i^2 - 4{,}288N_i + 2{,}037] \quad \text{(A20)}$$

$$(Me_{6S})_i \approx \frac{1}{4}\rho^2[285N_i^4 - 1{,}403N_i^3 + 3{,}595N_i^2 - 4{,}301N_i + 2{,}040] \quad \text{(A21)}$$

$$i \in [2, I-1]$$

$$(Me)_1 \approx \frac{1}{4}\rho^2[27N_i^4 - 266N_i^3 + 980N_i^2 - 1{,}602N_i + 981] \quad \text{(A22)}$$

3) Communications

$$Ce = \sum_{i=2}^{I} (Ce)_i \quad \text{(A23)}$$

$$(Ce)_i = 8\,[(N_{3S})_i\,(Ce_{3S})_i + (N_{4S})_i\,(Ce_{4S})_i + (N_{5S})_i\,(Ce_{5S})_i + (N_{6S})_i\,(Ce_{6S})_i] \quad \text{(A24)}$$

$$(Ce_{3S})_i \approx \rho^2[3N_i^2 - 3N_i + 1]^2 \quad \text{(A25)}$$

$$(Ce_{4S})_i \approx \rho^2[4N_i^2 - 5N_i + 2]^2 \quad \text{(A26)}$$

$$(Ce_{5S})_i \approx \rho^2[5N_i^2 - 8N_i + 4]^2 \quad \text{(A27)}$$

$$(Ce_{6S})_i \approx \rho^2[6N_i^2 - 12N_i + 8]^2 \quad \text{(A28)}$$

$$i \in [2, I]$$

where

$$N_i = 1 + (N - 1)/(2^{i-1});\ i \in [2, I] \quad \text{(A29)}$$

Figure Legend - Part One

Fig. 1 Globally minimized model, stiffness matrix population.

Fig. 2 Bandwidth expansion by substructuring row column placement.

Fig. 3 Multilevel edge-bisection of 3-D cube.

Fig. 4 Speedup for a 6 level edge-bisected tree.

Fig. 5 Speedup for a 5 level edge-bisected tree.

Fig. 6 Speedup for a 4 level edge-bisected tree.

Fig. 7 Speedup for a 3 level edge-bisected tree.

Fig. 8 Speedup for a 2 level edge-bisected tree.

Fig. 9 Memory reduction for a 6 level edge-bisected tree.

Fig. 10 Memory reduction for a 5 level edge-bisected tree.

Fig. 11 Memory reduction for a 4 level edge-bisected tree.

Fig. 12 Memory reduction for a 3 level edge-bisected tree.

Fig. 13 Memory reduction for a 2 level edge-bisected tree.

Fig. 14 Sequential processor assignment, and partially parallel single processor assignment.

Fig. 15 Partially parallel, multiple processor assignment.

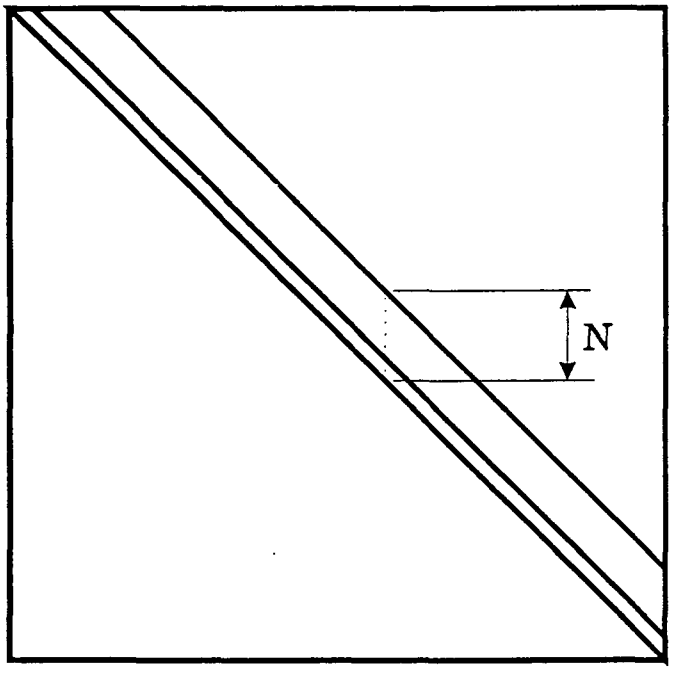

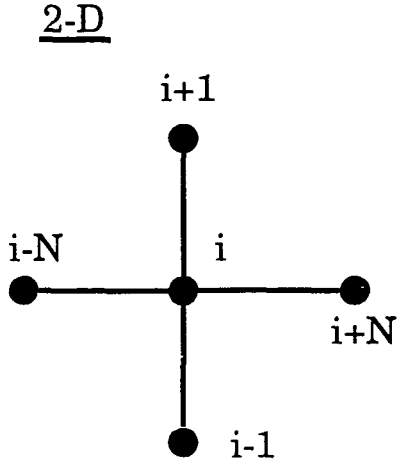

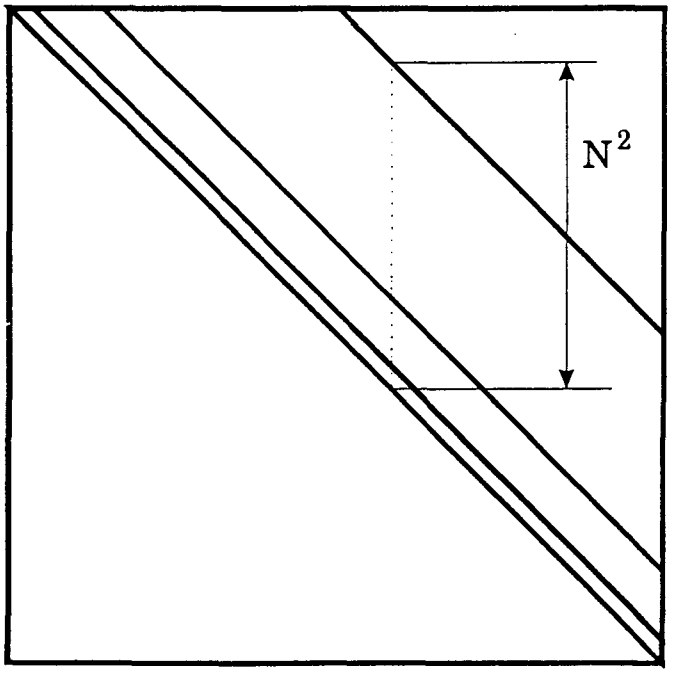

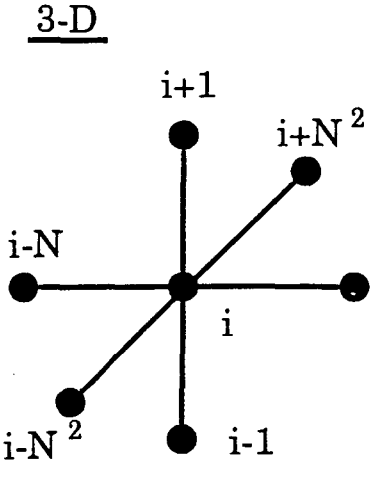

Figure 1

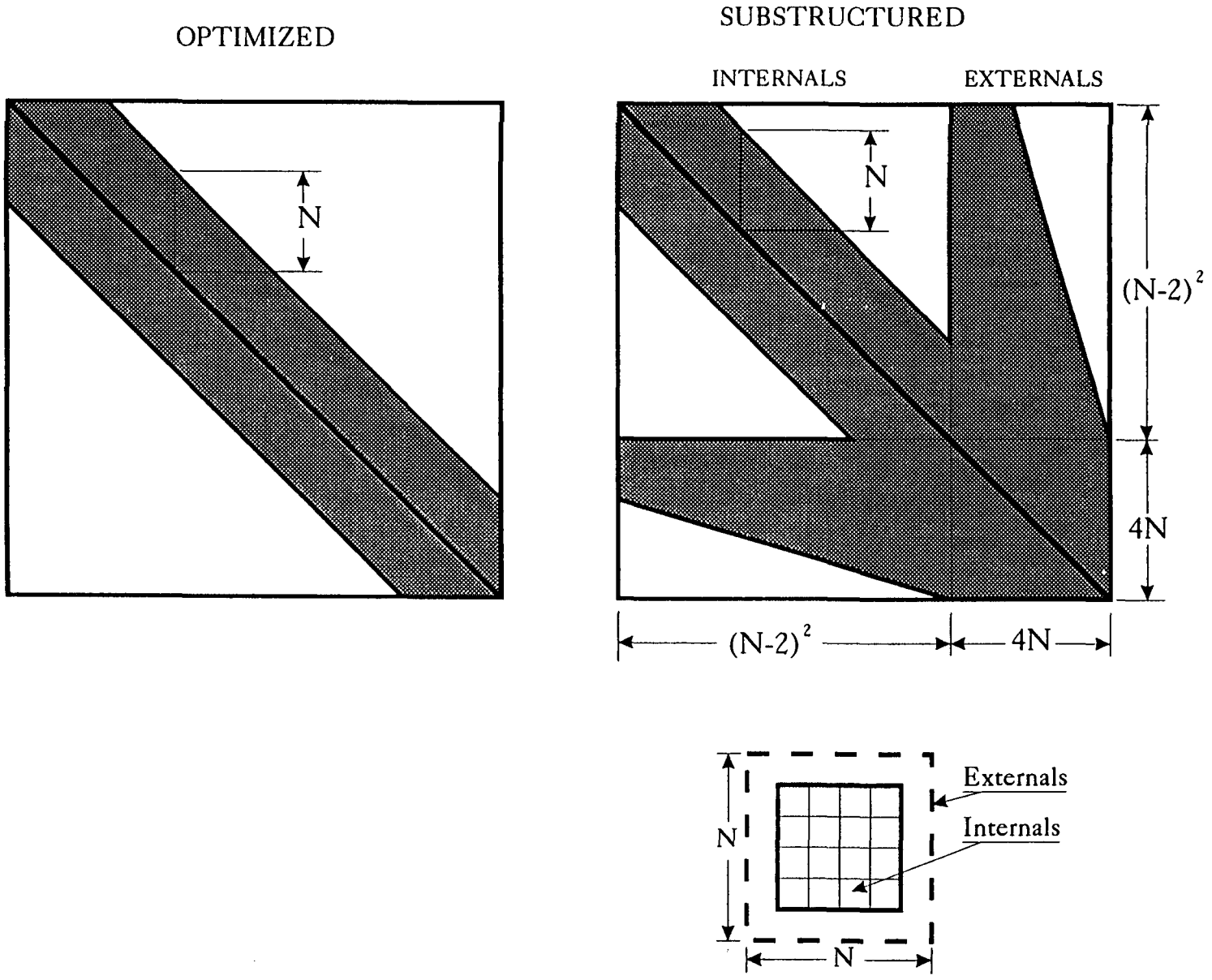
OPTIMIZED
N
SUBSTRUCTURED
INTERNALS
EXTERNALS
N
(N-2)²
4N
(N-2)²
4N
Externals
Internals
N
N

Figure 2

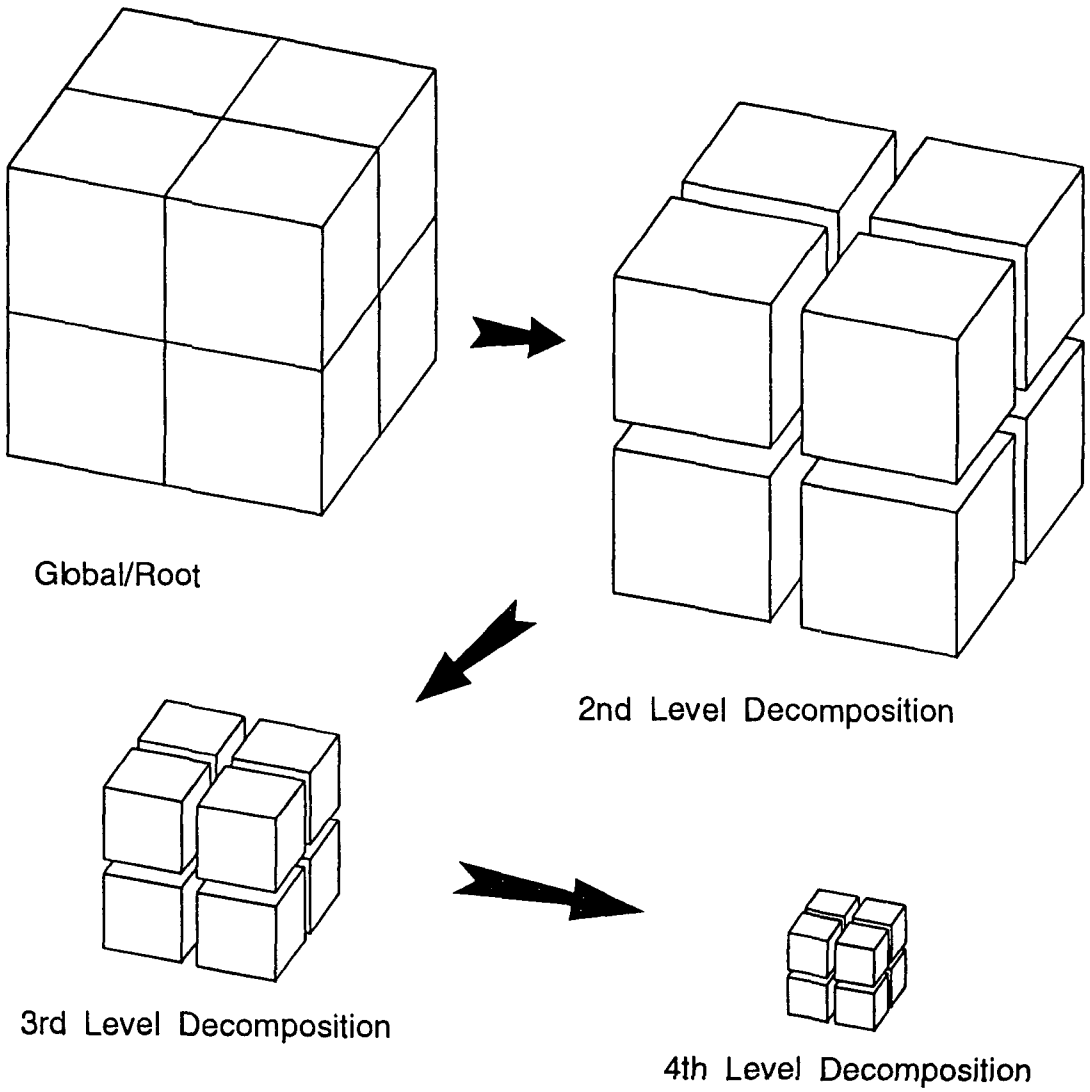
Global/Root
2nd Level Decomposition
3rd Level Decomposition
4th Level Decomposition

Figure 3

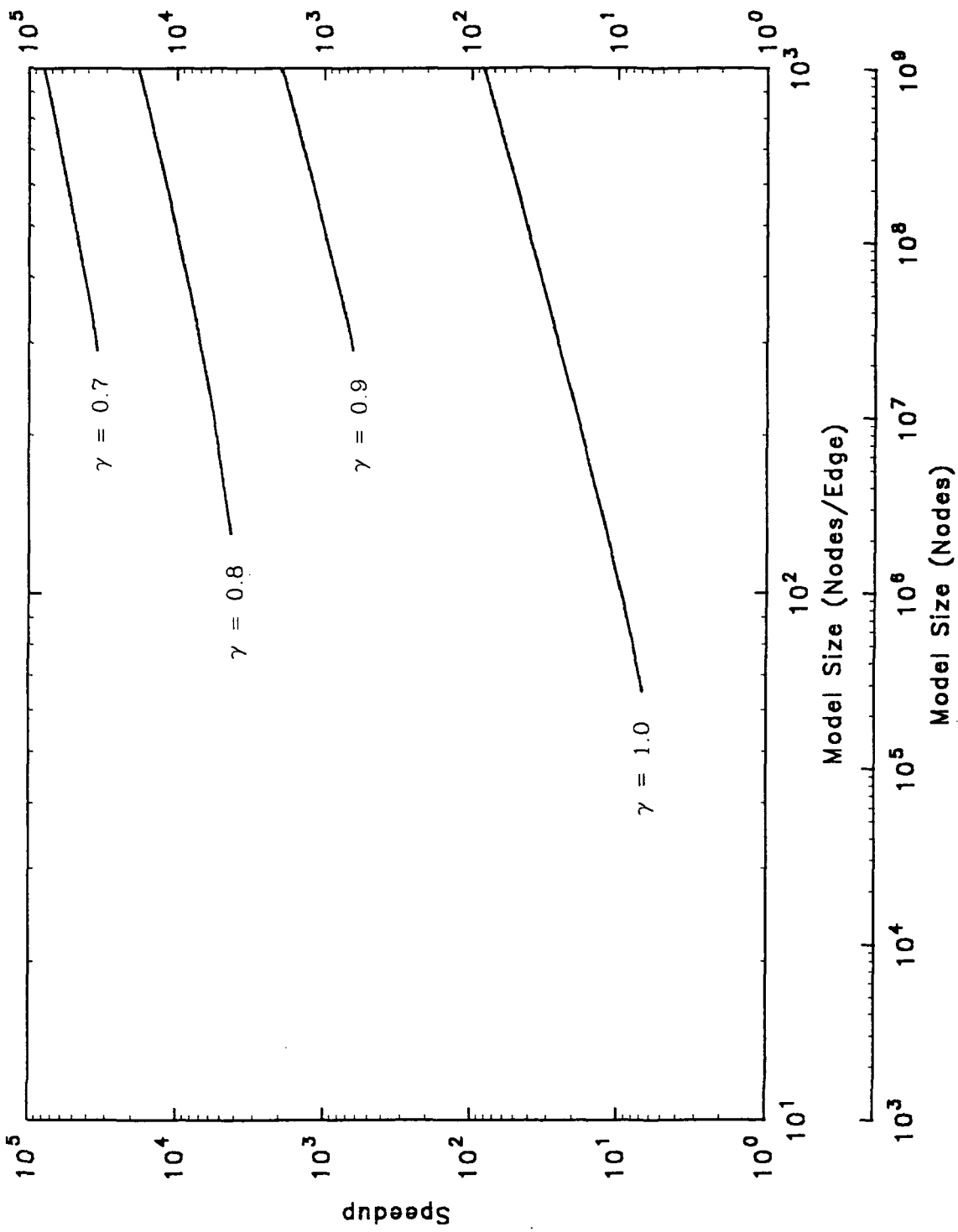
Speedup
Model Size (Nodes/Edge)
Model Size (Nodes)
γ = 0.7
γ = 0.8
γ = 0.9
γ = 1.0

Figure 4

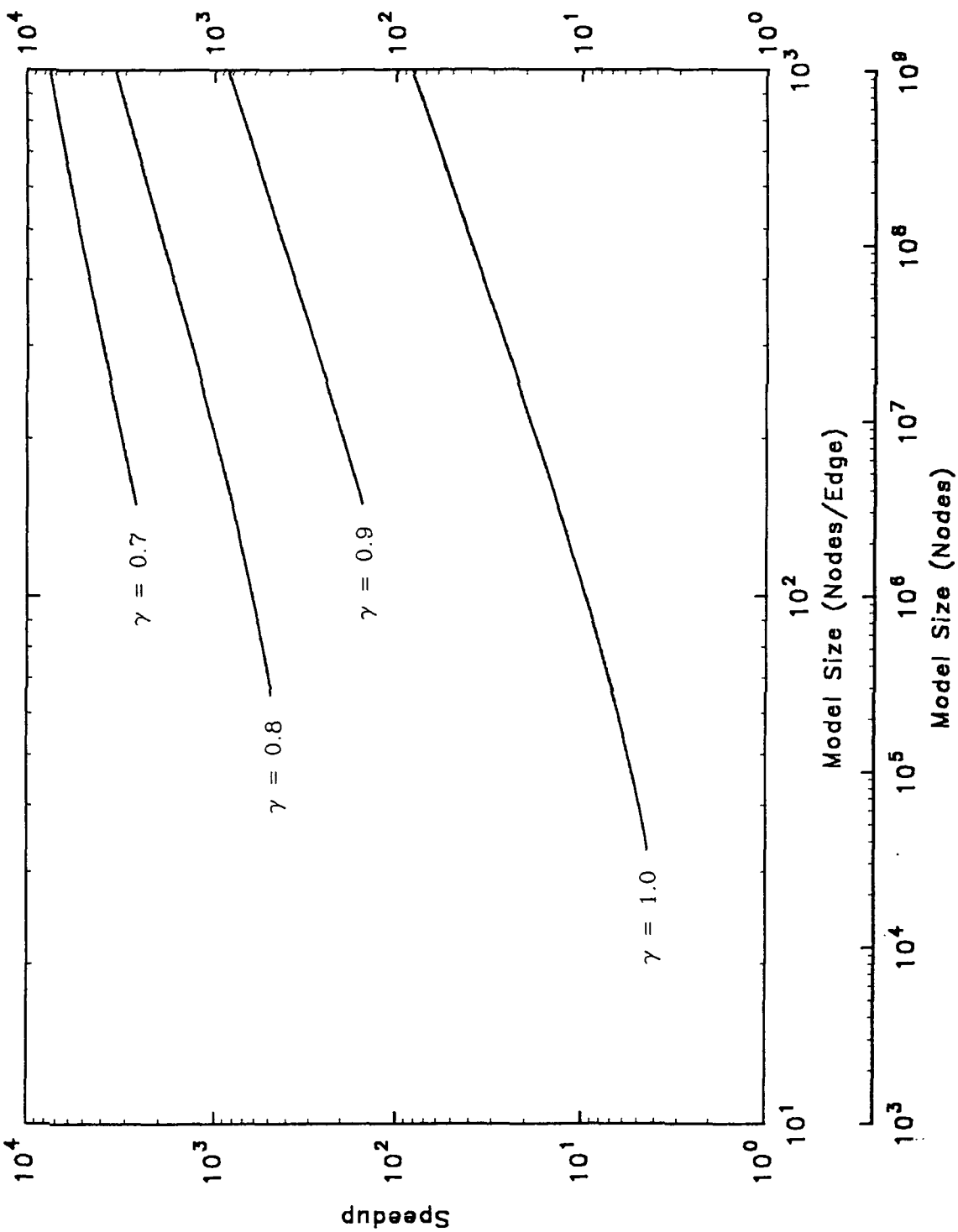
Speedup
Model Size (Nodes/Edge)
Model Size (Nodes)
γ = 0.7
γ = 0.8
γ = 0.9
γ = 1.0

Figure 5

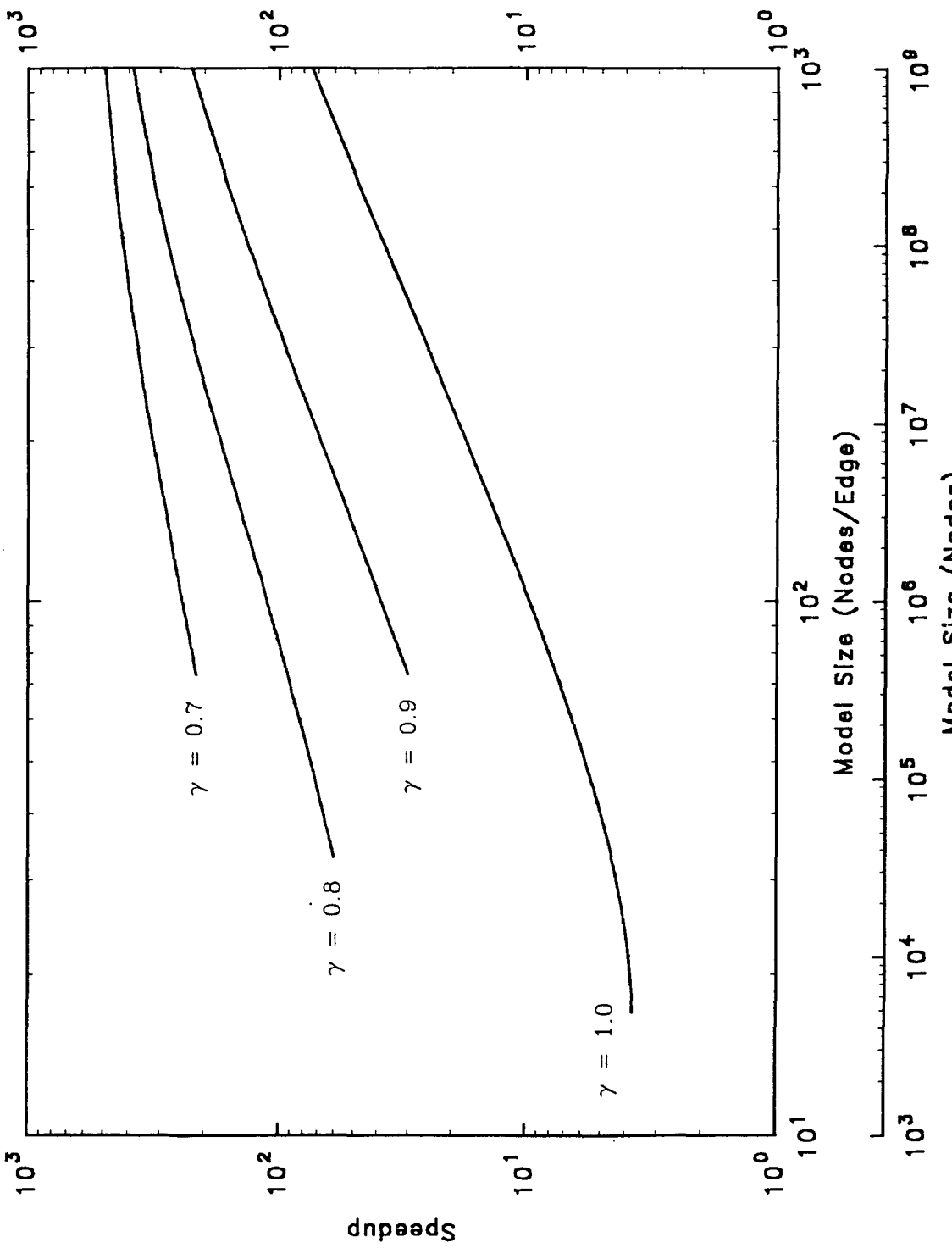
Speedup
Model Size (Nodes/Edge)
Model Size (Nodes)
γ = 0.7
γ = 0.8
γ = 0.9
γ = 1.0
10^0
10^1
10^2
10^3
10^4
10^5
10^6
10^7
10^8

Figure 6

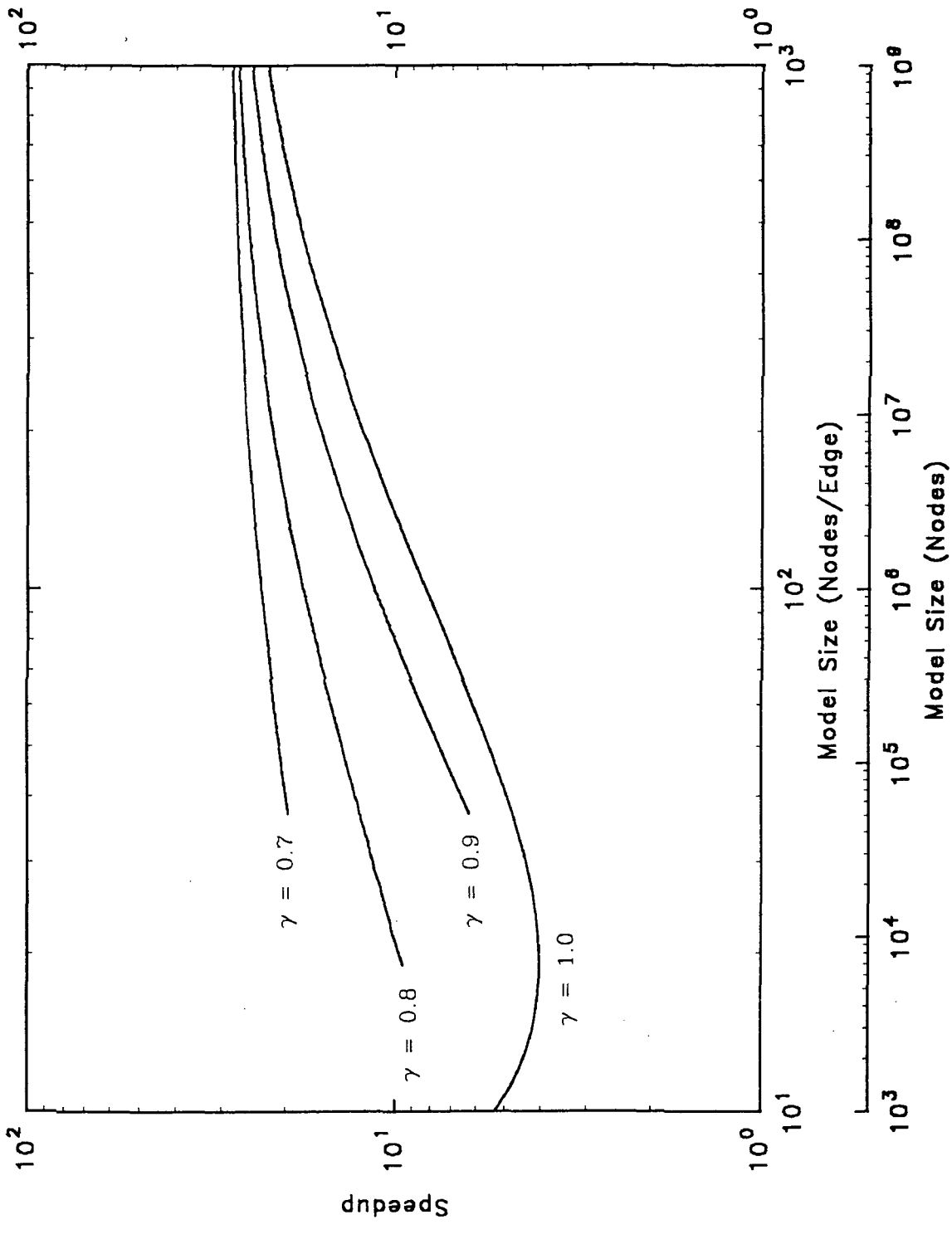
Speedup
Model Size (Nodes/Edge)
Model Size (Nodes)
γ = 0.7
γ = 0.8
γ = 0.9
γ = 1.0

Figure 7

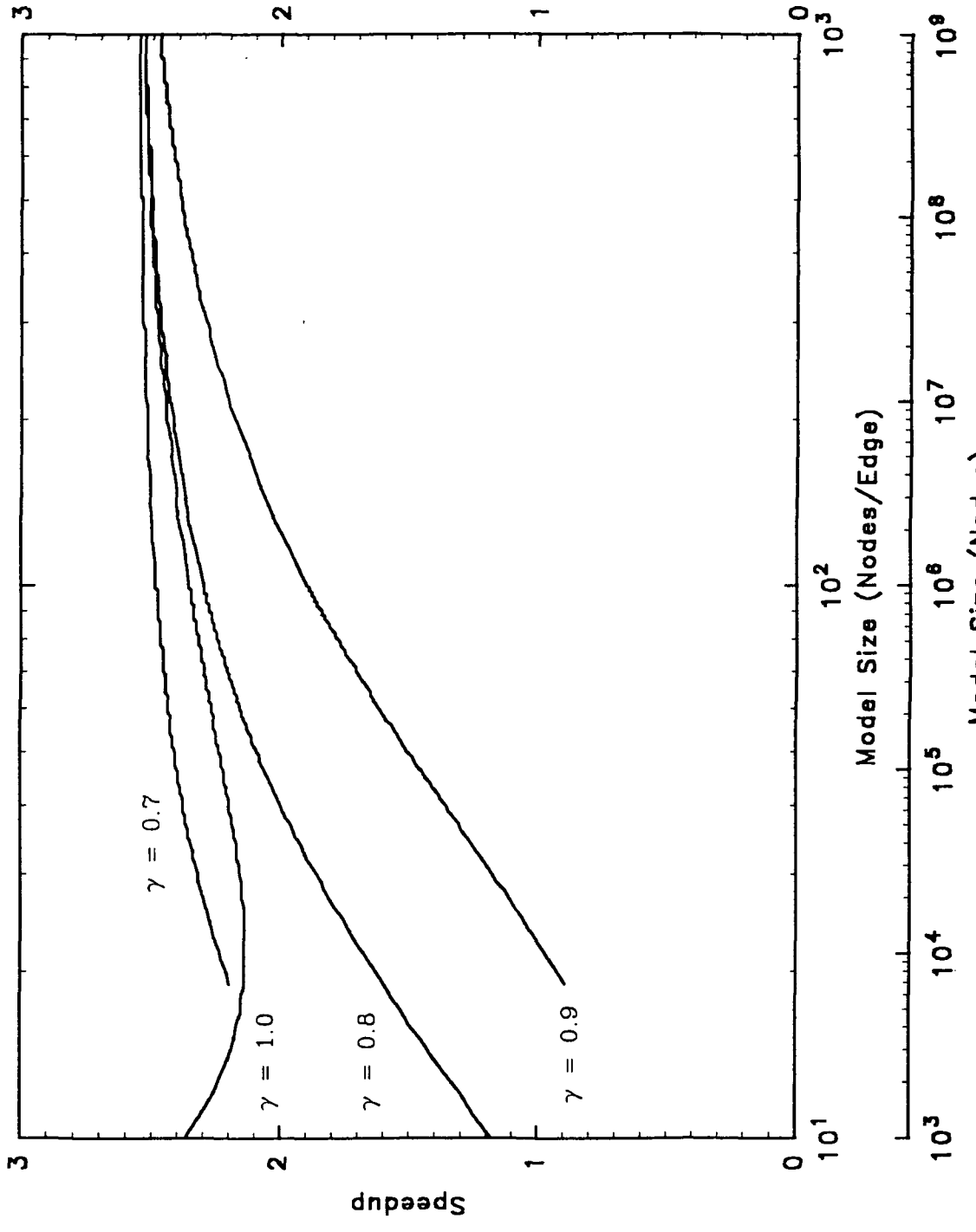
Speedup
Model Size (Nodes/Edge)
Model Size (Nodes)
γ = 0.7
γ = 1.0
γ = 0.8
γ = 0.9
0
1
2
3
10^1
10^2
10^3
10^4
10^5
10^6
10^7
10^8
10^9

Figure 8

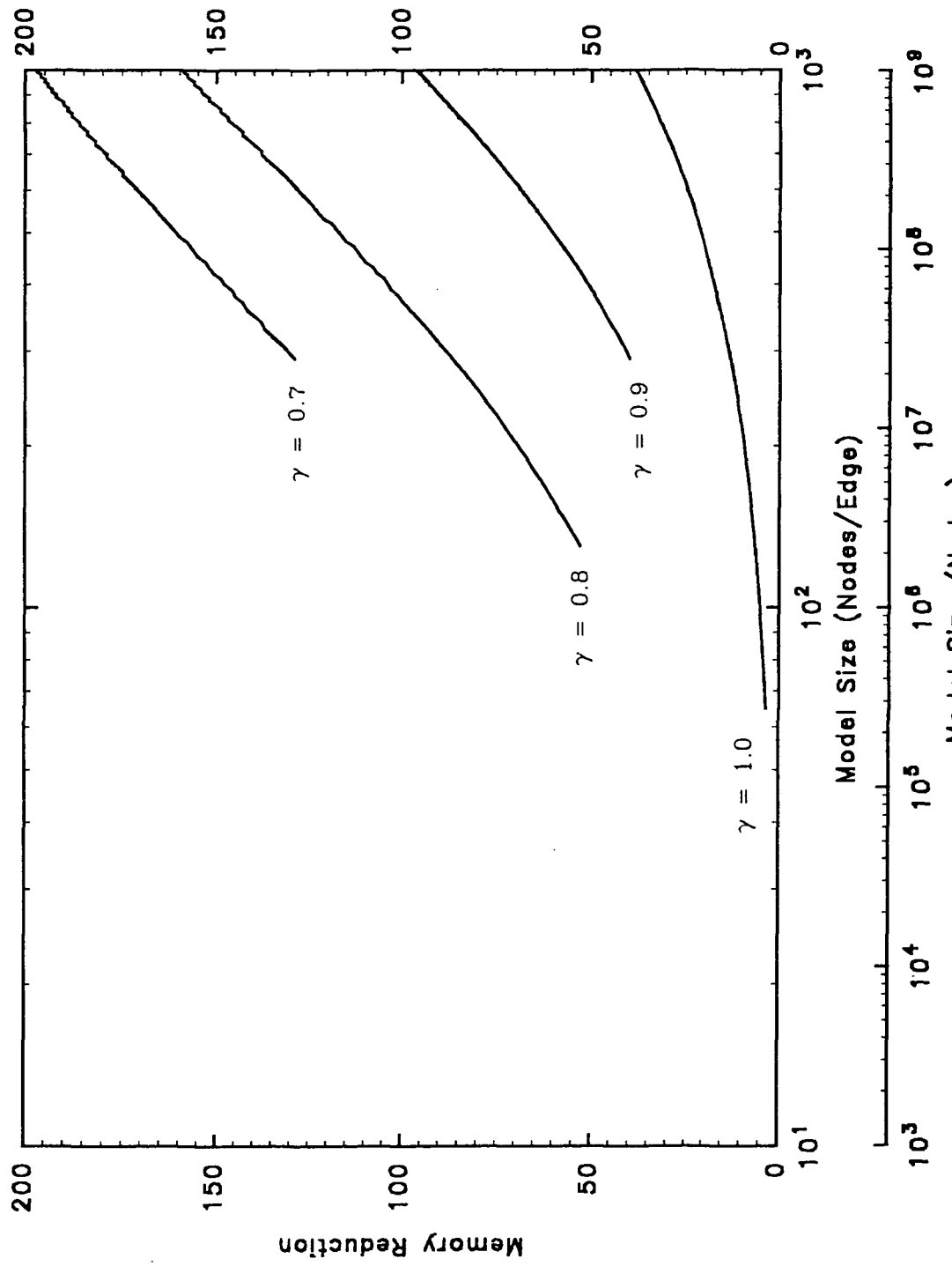
Memory Reduction
200
150
100
50
0
10^1
10^2
10^3
Model Size (Nodes/Edge)
10^3
10^4
10^5
10^6
10^7
10^8
10^9
Model Size (Nodes)
γ = 0.7
γ = 0.8
γ = 0.9
γ = 1.0

Figure 9

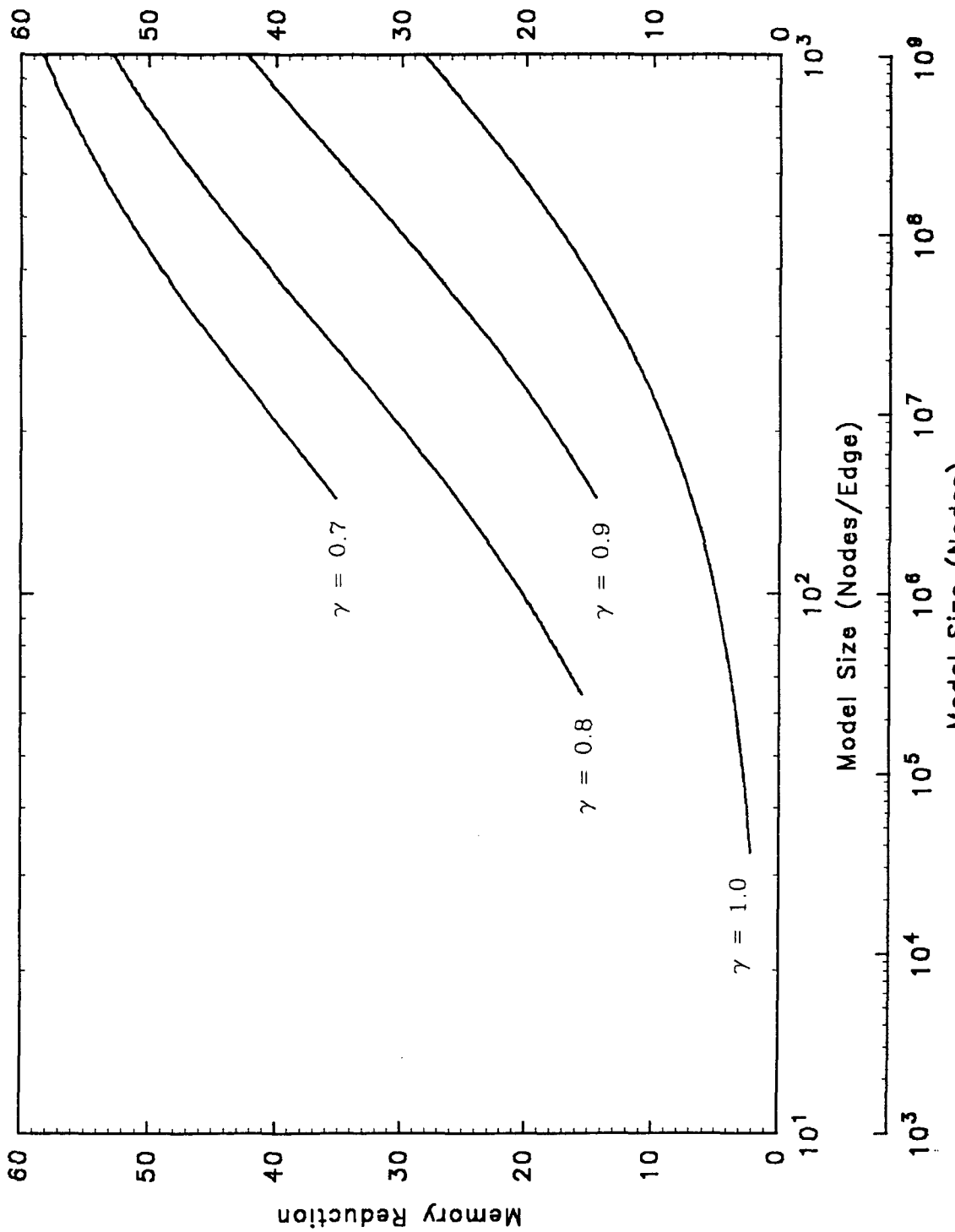
Memory Reduction
60
50
40
30
20
10
0
10^1
10^2
10^3
Model Size (Nodes/Edge)
10^3
10^4
10^5
10^6
10^7
10^8
10^9
Model Size (Nodes)
γ = 0.7
γ = 0.8
γ = 0.9
γ = 1.0

Figure 10

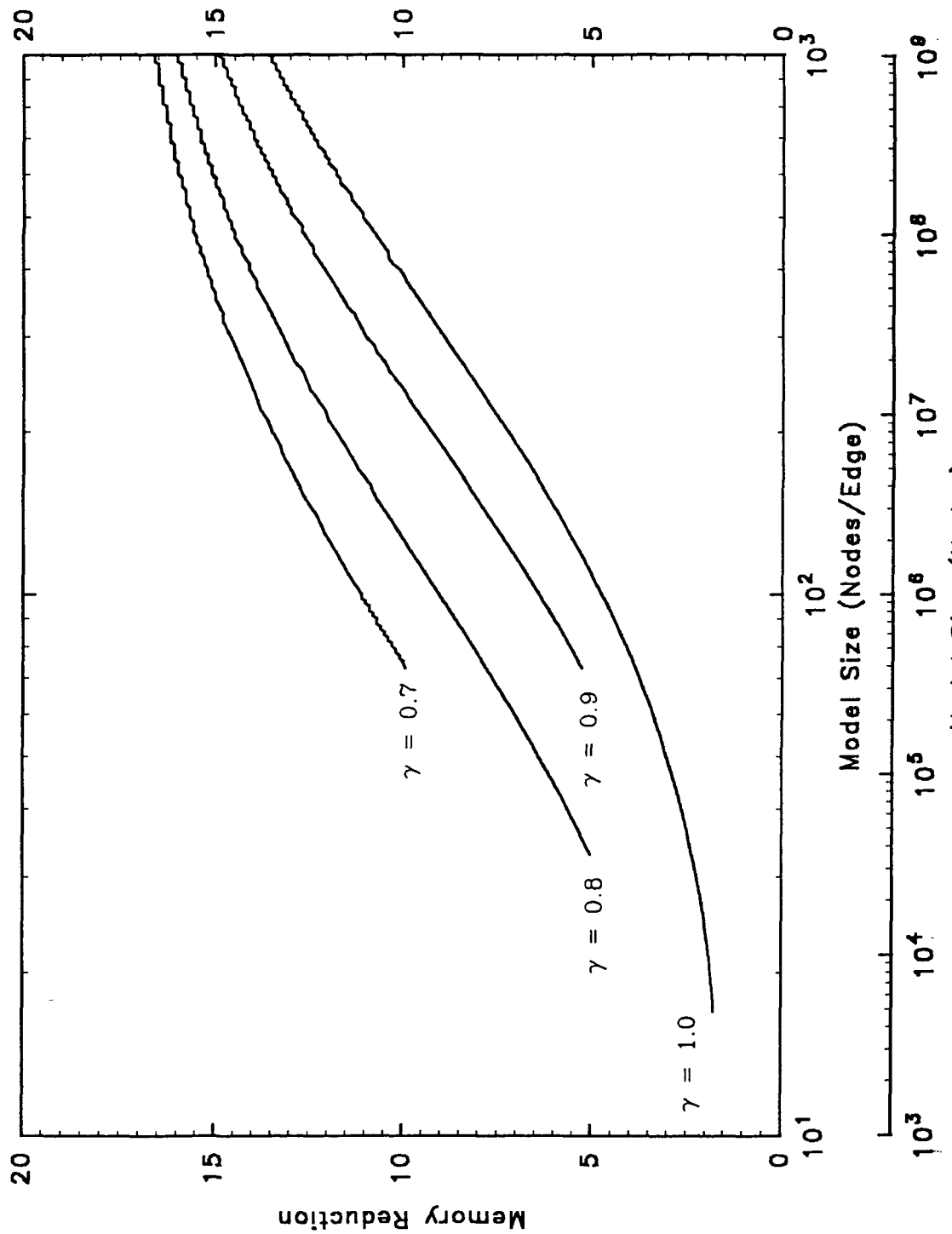
Memory Reduction
20
15
10
5
0
γ = 0.7
γ = 0.8
γ = 0.9
γ = 1.0
10^1
10^2
10^3
Model Size (Nodes/Edge)
10^3
10^4
10^5
10^6
10^7
10^8
10^9
Model Size (Nodes)

Figure 11

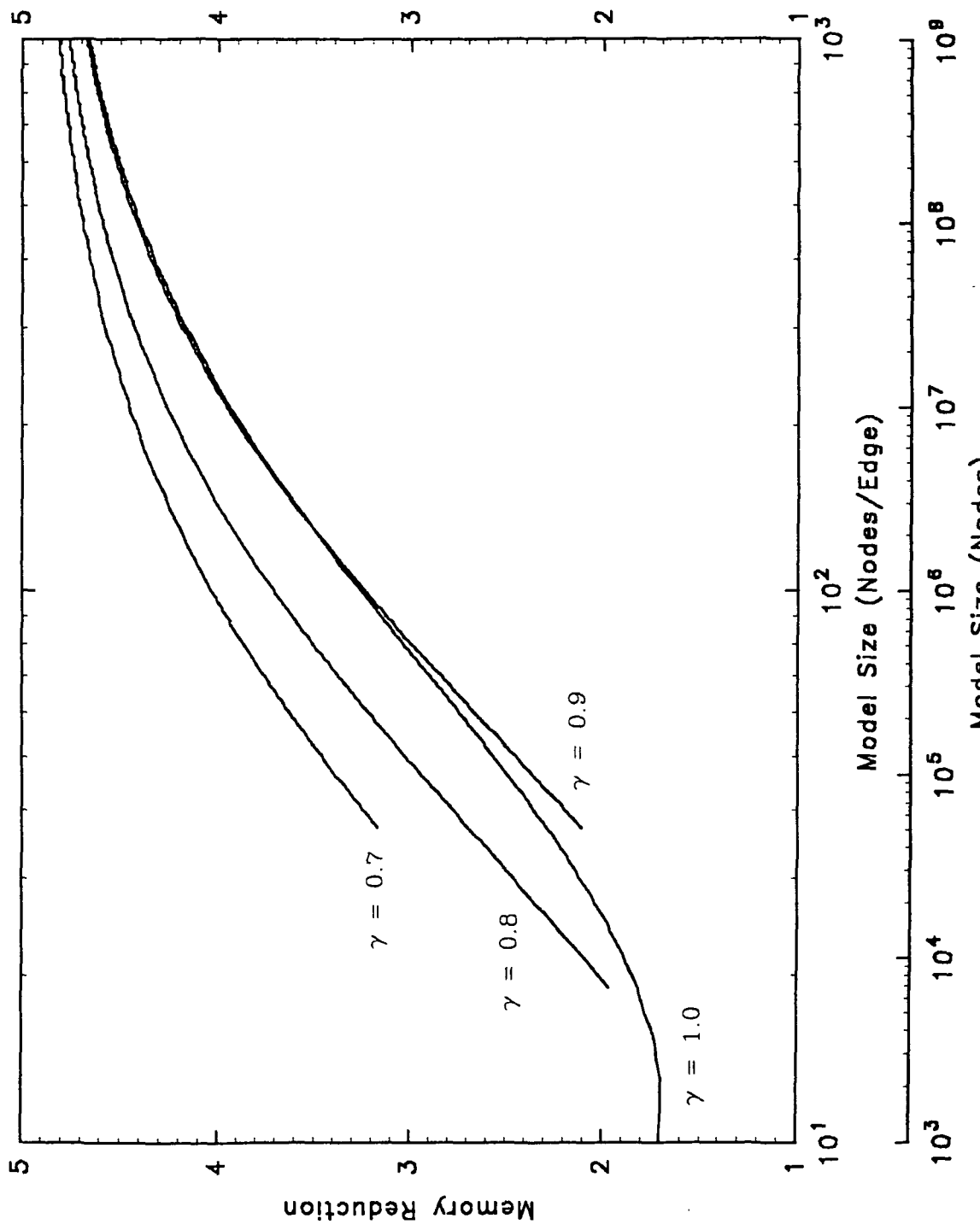
Memory Reduction
Model Size (Nodes/Edge)
Model Size (Nodes)
γ = 0.7
γ = 0.8
γ = 0.9
γ = 1.0
1
2
3
4
5
10^1
10^2
10^3
10^4
10^5
10^6
10^7
10^8
10^9

Figure 12

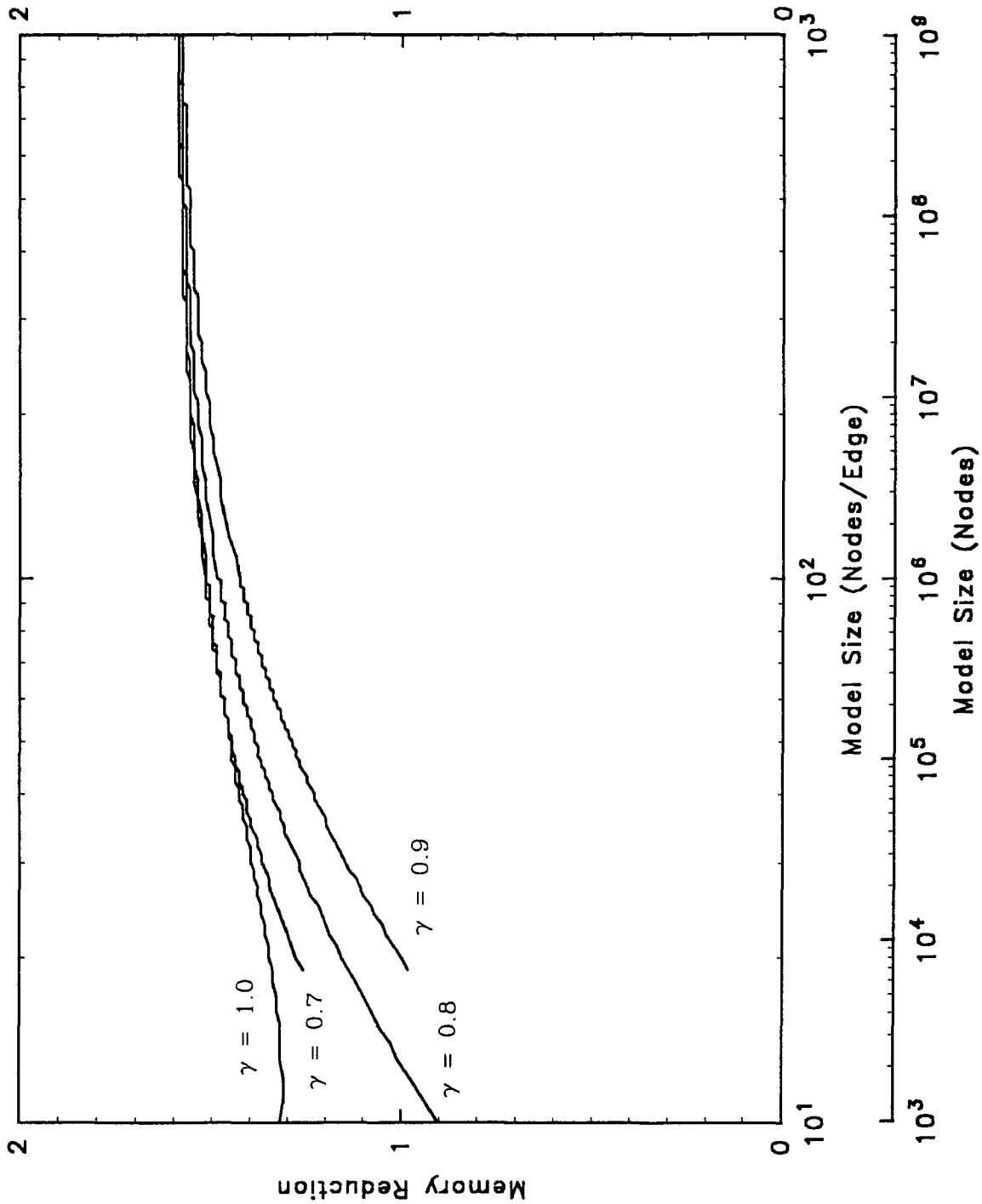
Memory Reduction
2
1
0
γ = 1.0
γ = 0.7
γ = 0.8
γ = 0.9
10^1
10^2
10^3
Model Size (Nodes/Edge)
10^3
10^4
10^5
10^6
10^7
10^8
10^9
Model Size (Nodes)

Figure 13

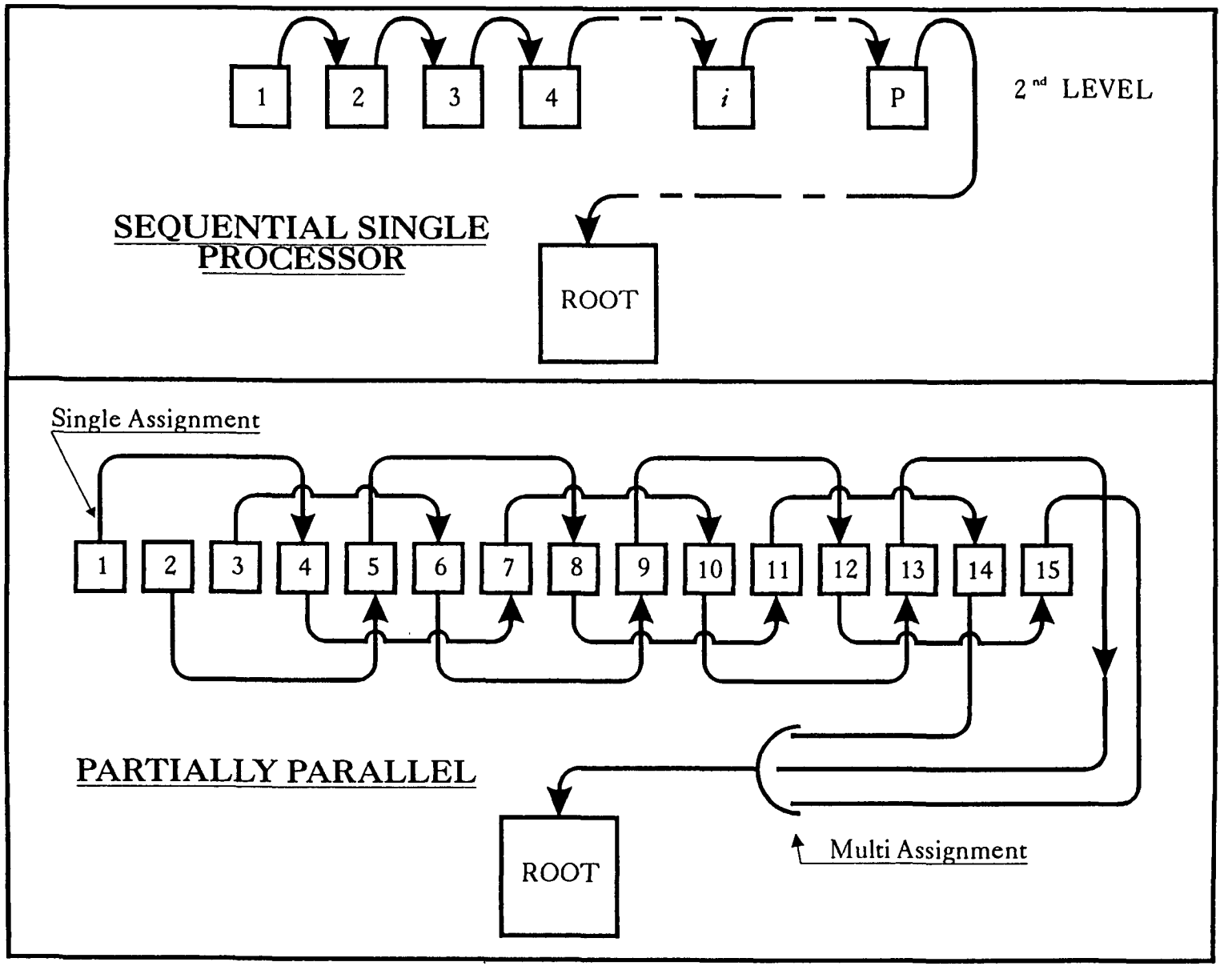
1
2
3
4
i
P
2nd LEVEL
SEQUENTIAL SINGLE PROCESSOR
ROOT
Single Assignment
1
2
3
4
5
6
7
8
9
10
11
12
13
14
15
PARTIALLY PARALLEL
ROOT
Multi Assignment

Figure 14

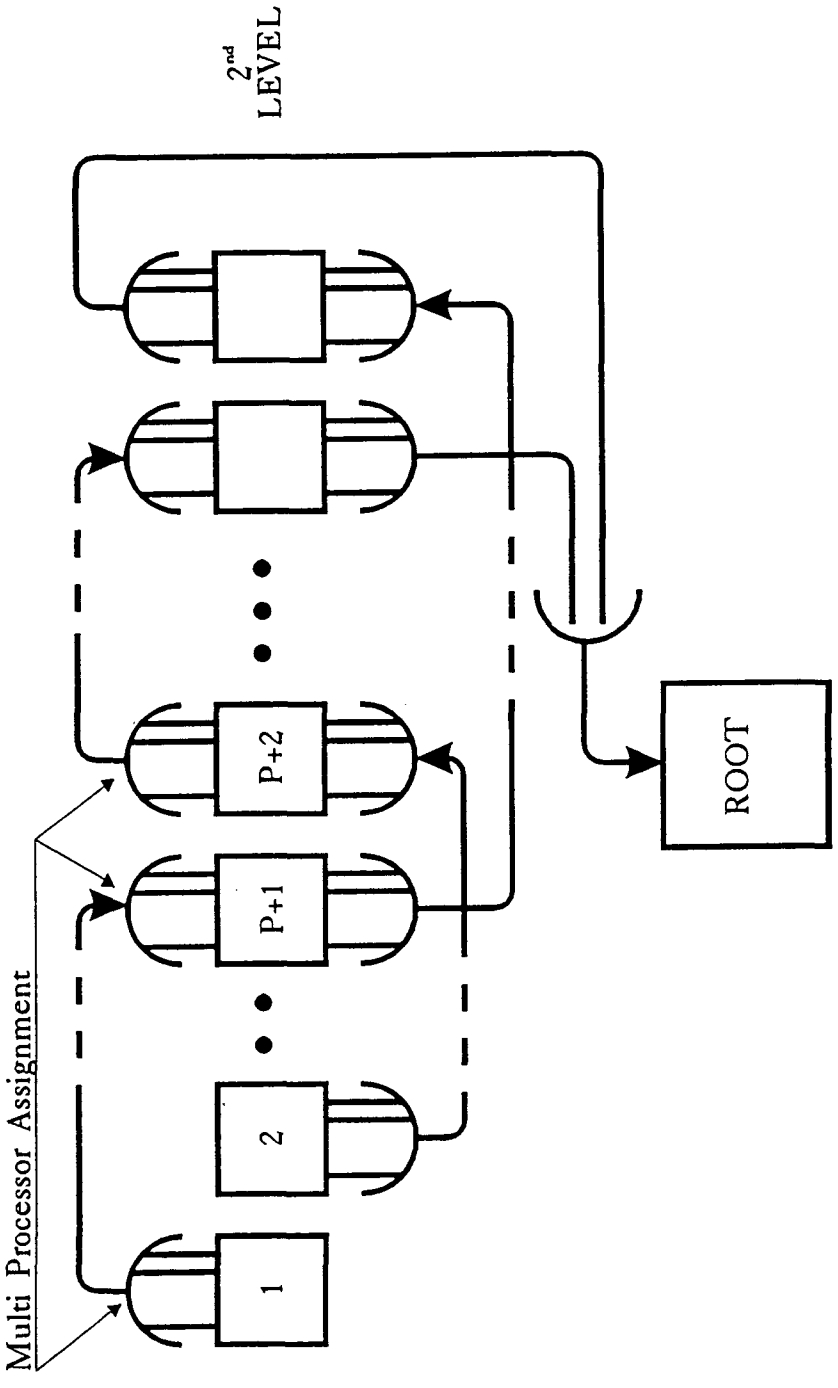

Figure 15

Hierarchically Partitioned Solution Strategy For CFD Applications: Part II - Numerical Applications

Joe Padovan[Δ]

[Δ]Departments of Mechanical and Polymer Engineering
The University of Akron
Akron, Ohio 44325-3903

Abstract

Part I of this series presented an analytical investigation of the use of HPT fluid simulations along with extensions to parallel computer environments. This was achieved in a closed form sense for simplified geometries. In Part II, the work will be numerically extended to handle more complex geometric morphologies. Specifically, the structure of the tree is optimized numerically contingent on problem dependent resource requirements. This is followed up with the results of several comprehensive implicit CFD simulation studies which demonstrate the effectiveness of the HPT concept.

1 Introduction

This part of the sequence presents the results of research in the area of parallel computer processing with Computational Fluid Dynamic (CFD) applications. The concept of Hierarchical Poly Trees (HPT) [1] is applied to prototypical CFD applications resulting in lower bound approximations to computational effort and memory requirements. Briefly stated, HPT implements multilevel substructural decomposition to achieve reductions in memory, computational effort, and communication requirements. For 2-D sequential problem formulations, the asymptotic upper bound trends show a square root of problem size reduction in effort and concomitantly, a fourth root reduction in memory requirements. In this context, as the model size increases, the HPT methodology shows increasing computer effectiveness in terms of both memory and computational effort. The HPT methodology extends this sequential performance improvement to the parallel processing environment in such a natural way that system overhead is minimized. Additionally, the HPT can be employed at the modeling stage, i.e. a preprocessor capable of taking advantage of, and indeed simplifying, modeling tasks such as geometric cell cloning, a feature associated mesh enrichment (FAME) [2] etc. We will show the optimal HPT to be dependent on the geometric features of the model. Once the HPT has been optimized (OHPT), it is not necessary to perform this task again and can be saved for future use. Hence, libraries of Optimized Hierarchical Polytree substructures (LOHPTS) can be developed. The HPT methodology is general enough to be applied to existing FD/FV/FEM CFD codes without an extensive rewriting of code and can be implemented on existing parallel computer architectures. OHPTs have additional benefits of being able to reconfigure parallel computing resources in a problem dependent optimal arrangement, something that other parallel computing strategies lack.

The sections that follow will provide: 1) a brief discussion of the CFD equations involved; 2) a numerical optimization scheme to define the tree structure for general problem geometric morphologies and; 3) its effects on parallelization. Included are the results of several large scale benchmark CFD applications. These illustrate the significant speedup potential and memory/communications reduction for typically sized incompressible flow models.

2 FE/FD Models - Implicit CFD Formulations

For discussion purposes consider the spatially discretized CFD system of equations of the general first order, nonlinear form;

$$[M]\ \frac{\partial\{v\}}{\partial t} + [K(v)]\ \{v\} = \{F\}, \tag{1}$$

where

$$\{v\} = \{v_1,\ v_2,\ v_3,\ p,\ T\}^T, \tag{2}$$

$[M]$ is the mass matrix, and $[K(v)]$ the nonlinear effective stiffness matrix. For a heat conducting incompressible fluid flow and either a FD or FE formulation [3], the general form of the stiffness matrix is given as,

$$[K(v)] = [K_c(v)] + [K_d] \tag{3}$$

The stiffness matrix is composed of $[K_d]$, a symmetric diffusion matrix, and $[K_c(v)]$, an unsymmetric convection matrix. In the primitive variable formulation, the symmetric diffusion matrix also contains the contributions from the pressure and the continuity equation. For discussion purposes, consider the two dimensional element for incompressible viscous fluid flow as used in the FE computer program ADINA-F [4,5]. This 9 node element is of second order in velocity and temperature, and linear in pressure to insure

stability via the Babuska-Brezzi condition [6,7]. Then the element mass and stiffness matrices are formed as,

$$[M] = \begin{bmatrix} [M_{11}] & & & \\ & [M_{22}] & & \\ & & [0] & \\ & & & [M_{44}] \end{bmatrix} \tag{4}$$

$$[K] = \begin{bmatrix} [K_{11}] & [0] & [K_{13}] & [0] \\ [0] & [K_{22}] & [K_{23}] & [0] \\ [K_{13}]^T & [K_{23}]^T & [0] & [0] \\ [K_{41}] & [K_{42}] & [0] & [K_{44}] \end{bmatrix} \tag{5}$$

A development of the submatrices $[M_{11}]$ and $[K_{ii}]$ can be found in Bathe [4,5]. Noting (5), the stiffness matrix is essentially full. This fullness of the stiffness matrix translates to large bandwidth and problem size. The velocity coupling terms $[K_{12}]$ and $[K_{21}]$ are equal to zero as a result of using the traditional Galerkin approach. In other formulations, these terms are not zero [8]. Also other coupling blocks, $[K_{14}]$ and $K_{24}]$, need not be zero [9]. In light of this, the most general formulation has a full element stiffness matrix. When the element matrices are assembled into the global stiffness matrix, a symmetric profile is created whose entries are not symmetric, i.e. $K_{ij} \neq K_{ji}$.

2.1 Steady State Formulation

The steady state formulation, obtained by dropping the partial time derivatives from (10) is then,

$$[K(v)] \{v\} = \{F\} \tag{6}$$

This nonlinear system is not directly solvable. Hence, an iterative procedure is the only method of solution. Typically successive substitution also known as fixed point iteration,

Picard iteration, or successive approximation is employed. Newton's method is generally relied on for problems with strong nonlinearities. This is a result of its asymptotic quadratic convergence rate. The application of Newton's method to (6) yields

$$\{v\}_{i+1} = \{v\}_i + [J]_i^{-1} \{\Psi(v_i)\} \tag{7}$$

where

$$[J] = \frac{\partial\{\Psi(v)\}}{\partial\{v\}} \tag{8}$$

In either case, matrix inversion is required. The solution to a steady state problem can also be given as the time asymptotic limit to an equivalent transient simulation. This approach is often preferred since it is history dependent and doesn't jump to different history dependent loading states.

2.2 Transient Formulation

After spatial semi-discretization (FD, FV, or FEM), all that is required for solution, is the resolution of the implicit temporal operator. This is accomplished in a variety of ways, e.g. the α method [10], predictor-corrector method [9], and other ODE solvers. The advantage of using high order ODE solvers, i.e. Gear's method, on the semi-discrete form, are negated by

- errors due to spatial discretization and
- nonlinear terms.

After the resolution of the temporal operator, the transient problem takes the form,

$$[K_D(v)] \{v\} = \{F_D\}, \tag{9}$$

where $[K_D(v)]$ is the dynamic stiffness matrix, and $\{F_D\}$ is the dynamic load vector. Thus a nonlinear set of equations, that resemble the steady-state formulation, must be solved at

each time step. For transient problems, each time step is chosen close enough to the previous one to use Newton's method. In practice, it has been found that it is desirable to control the error tolerance, such that a balance of one Newton iteration per time step is achieved. Let γ equal the HPT work reduction, then the resultant work effort for implicit transient solvers is γ times the work effort (Eff) prior to the application of the HPT methodology, i.e.

$$Eff_{HPT} = \gamma \, Eff \text{ (steady-state)} \tag{10}$$

$$Eff_{HPT} = \gamma \, Eff \text{ (transient)} \tag{11}$$

Thus the governing field equations have been reduced to solving repeatedly a large, sparse, unsymmetric system of implicit linear equations. Although we have illustrated the case of incompressible fluid flow, this also is true of compressible flow and more general continuum problems. With this in mind, we begin applications of the HPT methodology to four real world computational fluid dynamics models to benchmark the analytic results presented in Part I.

3 Application of the HPT Scheme to Real World CFD Applications

In Part I, we have shown analytically, via operations counts and symbolic algebra for square 2-D and cubic 3-D morphologies the HPT methodology capable of i) reducing the computational effort required for direct inversion of fluid simulations, ii) reducing the memory requirements, and iii) reducing the communications burdens. The analytics of the HPT methodology exhibit for a given model optional substructuring in terms of the number of levels and the number of substructures per level. In general arbitrary substructuring produces suboptimal results. Additionally the potential of the method to exploit coarse and fine-grained parallel computer architectures was briefly discussed.

It was necessary to base the analytic work on a regular (square and cubic) geometry to obtain a node numbering pattern to formulate analytic expressions of computational effort, memory and communications burdens. Real world models rarely have square or cubic morphologies. This led to the work of Padovan and Kwang who have automated the substructuring process [11]. Kwang's AUTOSUB program [12] numerically tallys the computational effort, memory and communications burden for arbitrarily shaped, multiply connected 2-D regions. The following sections of this paper discuss the application of the HPT methodology, outline the automated substructuring process and present four benchmark CFD applications to reinforce the analytic results presented in Part I.

The HPT process begins by hierarchically partitioning the model into multilevel substructures. Such a process is illustrated in Fig. (1). Typical of FD models, the double airfoil simulation described in Fig. (1) can be mapped into its topological equivalent, see Fig. (2). The overall process extends to more elaborate multibody grids, with more complex unit cells. Consider the modeling of the fluid flow around a stator blade cascade in the turbine section of a jet engine. Figure (3) illustrates a typical blade set, i.e., the first stator vane. Noting the periodicity, one can see that there is a recurring unit cell model. As can be seen from Fig. (3) the connectivity between cells consists of a row of repeated boundary nodes. This node row determines the root of the HPT. The second level branches are the unit cells. This is described in Fig. (4). Usually the cell is defined by many nodes. As a result, additional levels may be required to reduce the cell level computational effort, memory utilization and communications costs. For demonstration purposes, assume that the cell is a 2-D square. To balance the tree, we must decompose the cell into partitions which yield the minimum external/internal ratios. This is achieved for square zone shapes. Figure

(5) illustrates a typical multilevel partitioning of the cell to establish the zone sizes and number of levels, the Gaussian elimination process is relied on to determine the operations count. Since the forward matrix reduction phase requires the major effort, it is used to structure the tree architecture. Recall that the cell level requirements have been addressed in Part I of this paper.

Now the root level effort, memory and communications requirements can be determined. Recall that the root here consists of a cell interconnecting node row, i.e. Fig. (3.6). As a result of the forward elimination process performed at the branch levels, the condensed 'stiffness' linking the interconnecting nodes of the unit cells are fully populated. In this context, the root level assembly yields a matrix with a regular skyline height of $O(3\rho N_r)$ such that N_r denotes the number of upstream-downstream interconnect nodes at a given unit cell interface. Given N_c unit cells, the net size of the assembled root 'stiffness' is $2\rho N_r(N_c + 1)$. Hence the root level effort is

$$Fe(root) = 18\ \rho^3(N_c + 1)\ (N_r)^3 \tag{12}$$

The associated memory and communications requirements are defined by

$$Me(root) = 12\ \rho^2(N_c + 1)\ (N_r)^2 \tag{13}$$

$$Ce(root) = 16\ \rho^2\ N_c(N_r)^2 \tag{14}$$

Note, because of the regular form of the root of the blade cascade problem, reduction into its own HPT will not decrease its effort. Rather, to yield an improved tree, the only recourse is to agglomerate unit cells into larger repeated substructure. Such enlarged cells would then be treated in the same manner as before.

Employing (12-14) and the following expressions from Part I (15), (17), (21) we yield the following expression for the sequential formulation of the HPT associated with the cascade problem, namely

$$Fe(net) = Fe(root) + N_c Fe(unit\ cell) \tag{15}$$

$$Me(net) = Me(root) + N_c Me(unit\ cell) \tag{16}$$

$$Ce(net) = Ce(root) + N_c Ce(unit\ cell) \tag{17}$$

Optimization of the overall tree would follow as before. In the case that the root is treated as a single partition, then optimization would be performed only on the unit cell. In a later section, some trend studies will be overviewed to illustrate the benefits of the HPT.

3.1 Analytical-Numerical HPT Optimization

For problems composed of purely rectilinear cells, the foregoing development can directly handle the optimized structuring of the HPT architecture. In the case of more general forms of connectivity, an alternative approach must be employed. This of course is highly problem dependent. Generally, in fluids problems solved via the FD scheme, mesh connectivities are usually highly rectangular in nature. Hence, the associated HPT can be developed in a manner similar to that employed for the above noted turbine blade row problem. In contrast, FE meshes generally lead to relatively more complex nodal connectivities. This of course renders the direct analytical tinkering with the skyline too cumbersome an approach. To circumvent these difficulties, an alternative numerical procedure will be employed [11].

Overall the method consists of several phases of tree structuring, these include:

- phase 1; choose number of levels and branches per level.
- phase 2; decompose a given level into individual partitions.
- phase 3; bandwidth minimize internal degrees of freedom of each substructure.

- phase 4; compare performance characteristics of various parametrically varied tree configurations to establish optimal construct.

For the current purposes, a golden section search [13] methodology is employed to define the proper branch count for each level. In this method, the branching is not selected arbitrarily. Rather, it is defined through the golden ratio which is obtained from the appropriate Fibonacci sequence [13]. Alternatively, the Fibonacci search scheme [13] can also be employed. Here, it must be recognized that we are dealing with an integerized space. In this context, the search is rounded to the appropriate nearest integer value. To start the procedure, the overall external-internal degree of freedom ratio is used to define a rectangular region of like size. The HPT arising from the rectilinear model is then used to start the search. The central feature of the process is the automatic partitioning scheme. The main difficulty of partitioning is the need to establish the minimum external to internal ratio. Since mesh generation is prototypically geared to geometry and physical modeling needs, it is difficult to generalize the process. To circumvent this situation, an incremental agglomerational process based on localized node connectivity will be employed. In particular the procedure consists of several operational steps, namely:

1. Seeding the starting point of agglomeration.
2. Adjoin neighboring nodes in successive waves of attachment.
3. Terminate attachment when present partition size is reached.
4. Bandwidth minimize partition just generated.
5. Subtract agglomerated substructure and determine next seeding point.
6. Repeat reseeding, agglomeration, local bandwidth minimization, and substructural subtraction until the prescribed number of partitions is reached.

Figures (3.8 and 3.9) illustrate the dissection process of a tube bundle. Both single and multiple seedings are illustrated. As noted, such operations are repeated for each branch of the given level.

The starting/seeding point about which the adjoining process is initiated, is chosen to be nodes with the least connectivity, i.e. outside corners existing either in the original mesh or in the reduced mesh resulting from several partition deletions. Since many such points may exist in both the original and successively reduced mesh, the optimal choice is through the use of bandwidth minimization, i.e. via Cuthill-McKee [14] or Gibbs-Poole-Stockmeyer [15]. In particular the lead node of the optimized connectivity is declared the seed point. As seen in Fig. (6), for symmetric structures, simultaneous seeding and agglomeration is possible.

Once the starting point is established, the adjoining process can begin. To preserve the maximum bandwidth compactness for the given partition, the map of directly connected nodes is used to agglomerate mesh in successive waves of attachment. This process is illustrated in Figs. (6 and 7). Several factors control the attachment process: 1) the number of degrees of freedom per node, ii) the connectivities of nodes neighboring an already attached zone, iii) the degree of connectivity a node has within a given partition, and iv) the number of degrees of freedom the partition has been configured to contain. The issue of the degree of attachment that a given node possesses, has great bearing on controlling the generation of salients on the boundary (planar, 3-D) of partitions. In complex multiply-connected geometries, i.e. possessing holes, the agglomeration process can become trapped in salients or branched configurations. In such situations, weakly attached nodes in such boundary

regions can be reattached to surrounding partitions provided a higher level of connectivity is generated.

Overall the process of partitioning is performed at each level for all associated branches. Once a given branch is completed, it is treated as a full structure at the next higher tree level. In particular, it is partitioned in the same manner in successive applications of the foregoing decomposition process.

4 Benchmark Applications

To illustrate the speedup potential of the HPT scheme, the results of several benchmark studies will be considered. These include:

1. harbor model
2. airfoil model-multiple cell
3. turbine blade models-multiple cells
4. tube bundle assembly

The numerical experiments were conducted on a vectorized IBM 3090-200 employing extended memory architecture to provide for more primary (i.e. paged) memory. The software created to automate the hierarchical substructuring of the mesh used a combination of Cuthill-McKee [14] and Gibbs-Poole-Stockmeyer [15] bandwidth minimization to both seed agglomeration as well as define optimal partition level node numbering. The direct solver used to effect the solution was based on the traditional Wilson [10] type LU decomposition scheme employing skyline storage. The scheme was reformulated to profile style elimination. This enabled a more efficient use of multiple processor assignment for parallel studies.

The main thrust of the empirical work is to determine the speedup potential afforded by the HPT. A second interest is to establish the effects of geometry and geometric and

node connectivity variations. In this context, several types of mesh and geometry configuration were considered, in particular,

- branched topologies (harbor model)
- periodically repeating unit cells (turbine model)
- multiply connected domains (tube bundle)
- problems involving complex transitions in mesh connectivity (tube bundle)

Note since various of the problems considered have rectilinear type unit cells, the capability of the auto-mesh partitioning scheme can be tested against theoretical results. To provide a fair evaluation of speedup, the HPT results are compared with the global model employing a combination of Cuthill-McKee [14] and Gibbs-Poole-Stockmeyer [15] type minimization.

Beyond just testing treed versus global formulations, such studies enabled a comparison between the traditional bandwidth minimization procedures and the current partitioned approach. As will be seen from the results which follow, each geometric and connectivity arrangement has its own generic so called optimal HPT, i.e. the OHPT. In particular, each distinct internal and external boundary configuration and concomitant mesh topology will have a unique OHPT which minimizes effort, memory and communications. It is possible that a given model might have several so called local OHPT. The analytical solution of such nonlinear problem posses a real challenge in optimization. Two examples to follow, illustrate the numerical solution to the problem of determining the OHPT.

4.1 Harbor Model: Branched Topology

For the first test, we shall consider the Charleston harbor model of Johnson et al [16]. Figure (8) illustrates the boundary-fitted coordinate system. The associated mesh connectivity is given in Fig. (9). Since branched multiple connected spaces tend to degenerate the

bandwidth minimization process, the problem provides a realistic assessment of the speedup potential. Based on the automatic optimal decomposition, Table (1) illustrates the OHPT for two and three level configurations. As can be seen, significant speedups are recorded for the sequential applications of the OHPT, i.e. 2.50 (2 level) and 5.31 (3 level). Employed in a coarse grained four processor environment, the IBM 3090-400, the respective speedups are 7.75 and 16.9. Overall, use of the OHPT enables a significant reduction in crunch time. Concomitantly, the savings in storage obtained was a factor of 2.37 for the three level tree. Recalling the square topology asymptotic speedup and memory reduction, it follows that for the sequential case, memory reduction and speedup are proportioned by the relationship

$$\text{Memory Reduction} = O\left\{\sqrt{\text{speedup}}\right\} \tag{18}$$

As these savings are size dependent, the method generates improved performance with increasing problem size.

4.2 Airfoil Model: Multiply Connected Unit Cell

To simplify the modeling scheme, we will employ the traditional slender body mapping technique to determine the airfoil model [17]. Figure (10) illustrates the foil simulation and the topology of its node interconnection. Based on the noted configuration, Fig. (11) gives the speedup potential for various two level HPT structures. As can be seen, there are several local minima leading to relative OHPT. Overall, the global OHPT yielded a sequential speedup of 4.62 for the case of a four airfoil stack. For the three level tree, a speedup of 11.8 was recorded. The significant improvement between the two and three level trees is a result of the better balance between the internal and external variables. In particular, the two level tree has:

1. a more congested root with a larger bandwidth, and

2. top branches with a higher computational burden.

The extra level in the three level tree enables the root load to be spread out over more branch levels. Furthermore the top of the tree can be reduced into smaller partitions thereby reducing effort at that level. Note, for the given size configuration, no further improvement is possible since the procedure ran out of model to dissect. Employing coarse grained (four processor) parallelism, a speedup of 36.2 was recorded.

4.3 Turbine Blade Model: Multiply Connected Cells

The turbine blade cascade problem will be handled via cells developed employing either thin or blunt body mappings [17]. Here, the blunt body mapping will be employed. Considering the four blade assembly given in Fig. (3), several combinations of branch count yielded local OHPT. These are noted in Table (2). The optimal HPT (OHPT) yielded a speedup of 13.13 for the purely sequential three level case. Employed in a four processor parallel format, a 39.1 speedup was generated. To yield an even greater optimality, a four level tree was considered. This yielded an improvement of 17.59. As seen earlier, continued dissection saturates in effectiveness for a given problem size. In a similar context, increases in the number of levels also tends to yield asymptotic improvement ratios which are size dependent. This limit increases with problem size, refer to Discussion and Conclusions section.

4.4 Tube Bundle Assembly:

Multiply Connected Multi-Transition Model

Figure (12) illustrates the geometry of the tube bundle configuration employed to establish the effects of transitions in mesh connectivity on the effectiveness of the HPT. To handle the cylindrical to rectangular internal morphological variations, an FE type simulation is

employed. This leads to the $15k^+$ node mesh given in Fig. (12). Employing the automatic substructuring scheme, a complex arrangement of substructure is obtained. Figure (13) illustrates the local morphology of each second level branch. Here, only single point seeding was employed. As can be seen, a wide variety of partition shapes is obtained. This is a direct result of the varying mesh densities. As in all the preceding situations, the bundle arrangement had a preferred branch configuration. Considering a three level tree, a sequential speedup of 8.9 was obtained. The associated memory reduction was 2.9. Employed in a coarse grained four processor environment the speedup obtained was 28.7 relative to the single processor global solution.

5 Discussion and Conclusions

The numerical benchmark fluids applications presented in this paper have shown that the HPT methodology can generate order of magnitude improvements for modest sized problems. In the case of relatively square morphologies, as problem size becomes very large, the following asymptotic, many orders of magnitude, effort and memory reductions occur for sequential computer environments, namely:

$$S \sim O\{(\text{Problem Size})^{1/2}\} \tag{19}$$

$$M_r \sim O\{(\text{Problem Size})^{1/4}\} \tag{20}$$

Similar trends apply for the communications requirements. In a course grained parallel computing environment, where processor leapfrogging is employed to handle the tree, the effort reduction is proportional to $E\ P$, namely

$$P\{S\} \sim O\{(\text{Problem Size})^{1/2}\}\ E\ P \tag{21}$$

Note since the Tree provides for individual updating of each of the top level branches, the model stiffness regeneration effort is reduced by the same factor ($E\ P$). Overall, the HPT forms a naturally parallelizable communications link. Since it minimizes memory and effort, hardware demands are also reduced. This is not the case with recent attempts at parallelizing direct global solvers, which leave the memory and effort requirements unchanged.

In fluid applications, models of such problems as flow over wings, turbine/compressor blades, nozzles and ducts, usually involve mesh connectivities which are mapped to the boundary geometry. Thereby, rectilinear mesh morphology, prototypical of FD models can be made to accommodate a variety of configurations. Observe that once an OHPT is derived for a given mesh morphology; all that needs to be saved, in a library for future use, is a map of nodal connectivities. Now, the speedup, memory and communications reductions are available for all future computer runs of the given model connectivity. This points to the development OHPT libraries of various recurring system components. Such an attribute is particularly useful in industrial environments, where design variations often involve only minor geometric perturbations. Additionally, the Tree structure facilitates such modeling tasks as geometric cell cloning. In particular, the unit cells can be treated as repeated branches of the Tree. This reduces the efforts associated with:

- mesh generation,
- mesh embedding,
- mesh updating, and
- condensation.

Only recently, the substructuring technique has been exploited for its inherent parallelism. Farhat and Wilson [18] implemented a two-level substructuring finite element code on a

32-processor hypercube. They reported significant reductions in computational effort and processor efficiencies less than unity, i.e. sublinear. This is because they ignored the optimality involved in the substructuring process, and arbitrarily equated the number of available processors to the number or substructures in the FE model.

A domain cannot be arbitrarily disected into substructures in which a number of processors are arbitrarily assigned to the substructures, and expected to yield optimal performance. In fact arbitrary dissection and processor assignment are most likely to lead to suboptimal or minimal performance. Another method for partitioning a FE model for a parallel computer environment, is the so-called Elimination Tree or Nested Dissection theory [19]. While the use of Elimination Trees may yield modest computational improvements, as with the traditional frontal and skyline schemes, such approaches become particularly awkward for self-adaptive refinement during the solution process. Moreover, advocates of this theory have stated that multilevel Elimination Trees have not yielded significant benefits [19]. This conclusion is a direct contradiction of the results reported by Furuike [20] and the results in this work.

T. Furuike in 1972 described a finite element computer program with multiple level substructuring capabilities. He concluded that a multilevel method can virtually eliminate large band, active column, sparse with wide band, etc. Matrices, resulting in a considerable decrease in central processing unit (CPU) time. His conclusions, drawn from only two examples, are somewhat misleading because not all assemblages of multilevel substructures lead to enhanced performance. He viewed the method as a serial processing technique for a multiuser computer environment, and did not develop any trends or insights into this process and didn't report any capability for parallel processing.

Practical considerations of available computer resources limit the total number of benchmark trials and restrict the benchmarks to 2-D models. A sufficient number of trials of 2-D benchmark real world CFD simulations presented here confirm the results and assumptions of the 2-D analytic investigation of the HPT methodology presented in Part I. In all, several hundred CPU hours in a mainframe environment were consumed in the trials. These results also tend to affirm the results of the 3-D analytic investigation (see Part I), since it was based on the same assumptions and methods. Thus the 3-D analytic trends should be useful in the aprior assessment of the 3-D HPT methodology which was the original intent of the 3-D analytic work.

Lastly, the HPT methodology applies both to FE and FD simulations, solid-fluid-thermal simulations as well as other multiphysics models.

References - Part Two

[1] J. Padovan, D. Gute and K. Johnson, Hierarchical Poly Tree Computer Architectures Defined by Computational Multidisciplinary Mechanics, Computers and Structures, Vol. 32, No. 5, pp. 1133-1163, 1989.

[2] C.M. Albone, An Approach to Geometric and Flow Complexity Using Feature-Associated Mesh Embedding (FAME): Strategy and First Results, Eds. K.W. Morton, and M.J. Baines, Numerical Methods for Fluid Dynamics and Aerodynamics III, Clarendon Press, pp. 215-235, 1988.

[3] O. Pironneau, Finite Element Methods for Fluids, Wiley, 1989.

[4] K.J. Bathe and Jian Dong, Solution of Incompressible Viscous Fluid Flow with Heat Transfer using ADINA-F, Computers and Structures, Vol. 26, No. 1/2, pp. 17-31, 1987.

[5] K.J. Bathe and Jian Dong, Studies of Finite Element Procedures - The Use of ADINA-F in Fluid Flow Analyses, Computers and Structures, Vol. 32, No. 3/4, pp. 499-516, 1989.

[6] I. Babuska and A.K. Aziz, Survey Lectures on the Mathematical Foundations of the Finite Element Method, Ed. A.K. Aziz, Mathematical Foundations of the Finite Element Method, Academic Press, N.Y., 1972.

[7] F. Brezzi, On the Existence, Uniqueness, and Approximation of Saddle-Point Problems Arising from Lagrange Multipliers, R.A.I.R.O. Numer. Anal., Vol. 8, pp. 129-151, 1974.

[8] M.D. Olson and S.Y. Tuann, Primitive Variables Versus Steam Function Finite Element Solutions of The Navier-Stokes Equations, Eds., R.H. Gallagher, O.C. Zienkiewicz, J.T. Oden, M.M. Cecchi, and C. Taylor, Finite Elements in Fluids, Vol. 3, Wiley, 1978.

[9] FIDAP Theoretical Manual, Fluid Dynamics International Inc., Evanston, Illinois, Jan., 1990.

[10] K.J. Bathe, Finite Element Procedures in Engineering Analysis, Prentice-Hall, Englewood Cliffs, N.J., 1982.

[11] J. Padovan and A. Kwang, Hierarchically Parallelized Constrained Nonlinear Solvers with Automated Substructuring, Computers and Structures, Vol. 41, pp. 7-33, 1991.

[12] A. Kwang, Hierarchical Poly Tree Configuration for Nonlinear Finite Element Solvers, Ph.D. Dissertation, University of Akron, January 1991.

[13] M.M. Denn, Optimization by Variational Methods, McGraw-Hill, N.Y., 1969.

[14] E. Cuthill and J. McKee, Reducing the Bandwidth of Sparse Symmetric Matrices, Proc. ACM National Conference, pp. 157-172, 1969.

[15] N.E. Gibbs, W.G. Poole, and P.K. Stockmeyer, An Algorithm for Reducing the Bandwidth and Profile of a Sparse Matrix, SIAM Journal of Numerical Analysis, Vol. 13, pp. 236-250, 1976.

[16] B.H. Johnson and J.F. Thompson, A Discussion of Boundary-Fitted Coordinate Systems and Their Applicability to the Numerical Modeling of Hydraulic Problems, Misc. Paper H-78-9, U.S. Army Engineer Waterways Experiment Station, Vicksburg, Mississippi, 1978.

[17] C.A.J. Fletcher, Computational Techniques for Fluid Dynamics, Vol. II, Springer-Verlag, N.Y. 1988.

[18] C. Farhat and E. Wilson, A New Finite Element Concurrent Computer Program Architecture, International Journal For Numerical Methods in Engineering, Vol. 24, 1987, pp. 1771-1792.

[19] A. George and J. Liu, Computer Solution of Large Sparse Positive Definite Systems, Prentice-Hall, Englewood Cliffs, N.J., 1981.

[20] T. Furuike, Computerized Multiple Level Substructuring Analysis, Computers and Structures, Vol. 2, 1972, pp. 1063-1073.

Figure Legend - Part Two

Fig. 1 Hierarchically partitioned FD model, multilevel substructures.

Fig. 2 FD model and its partition topology.

Fig. 3 Stator blade set.

Fig. 4 Unit cells of stator blade set.

Fig. 5 Multilevel cell partitioning.

Fig. 6 Automated partitioning via single point seeding.

Fig. 7 Automated partitioning via multipoint seeding.

Fig. 8 Charleston Harbor model, boundary-fitted coordinate system.

Fig. 9 Charleston Harbor model, associated mesh connectivity.

Fig. 10 Airfoil model, simulation and nodal interconnection topology.

Fig. 11 Airfoil model speedup potential for various two level HPT structure.

Fig. 12 Tube bundle assembly and mesh connectivity.

Fig. 13 Tube bundle assembly, second level branch morphology.

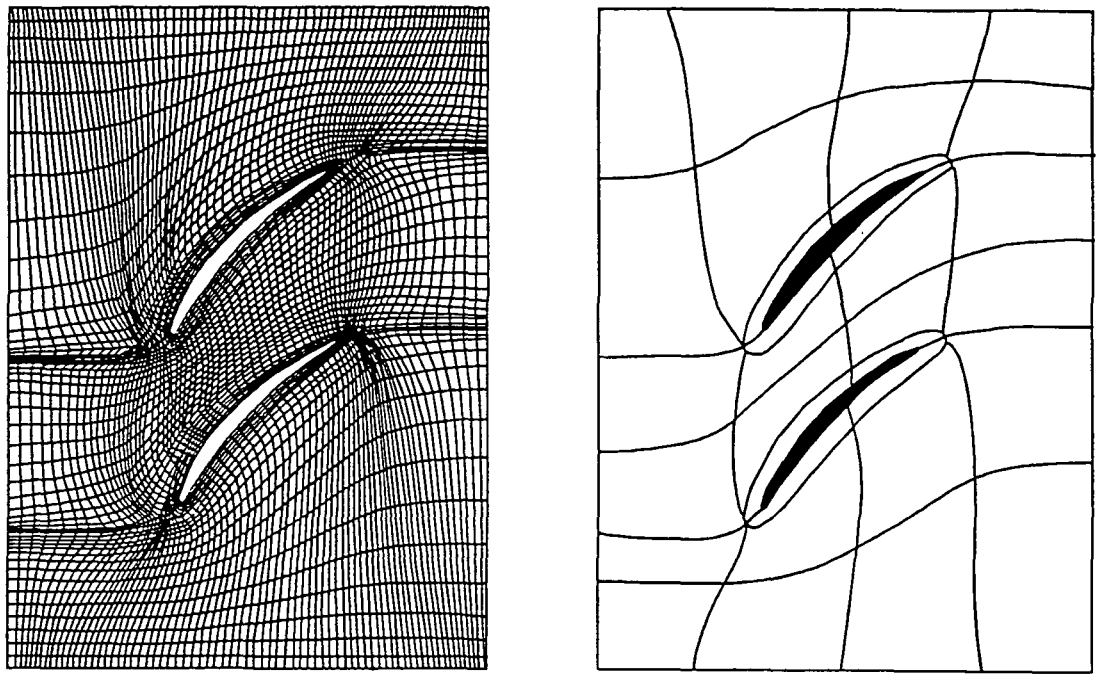

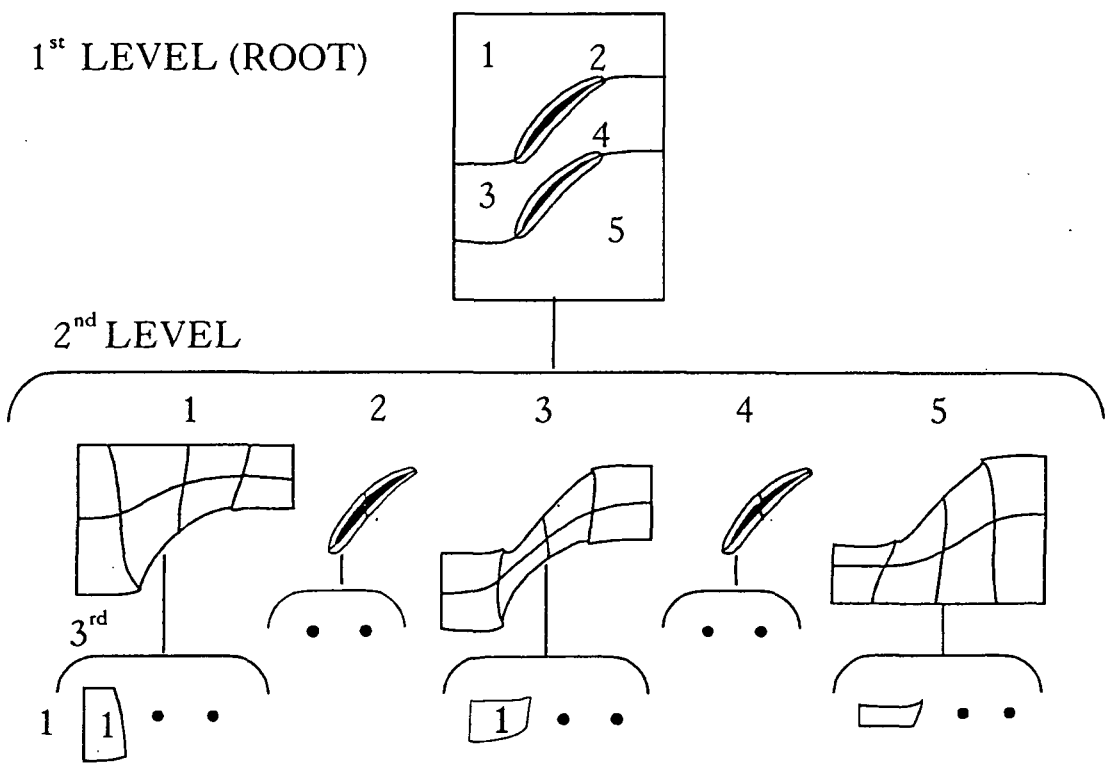

Figure 1

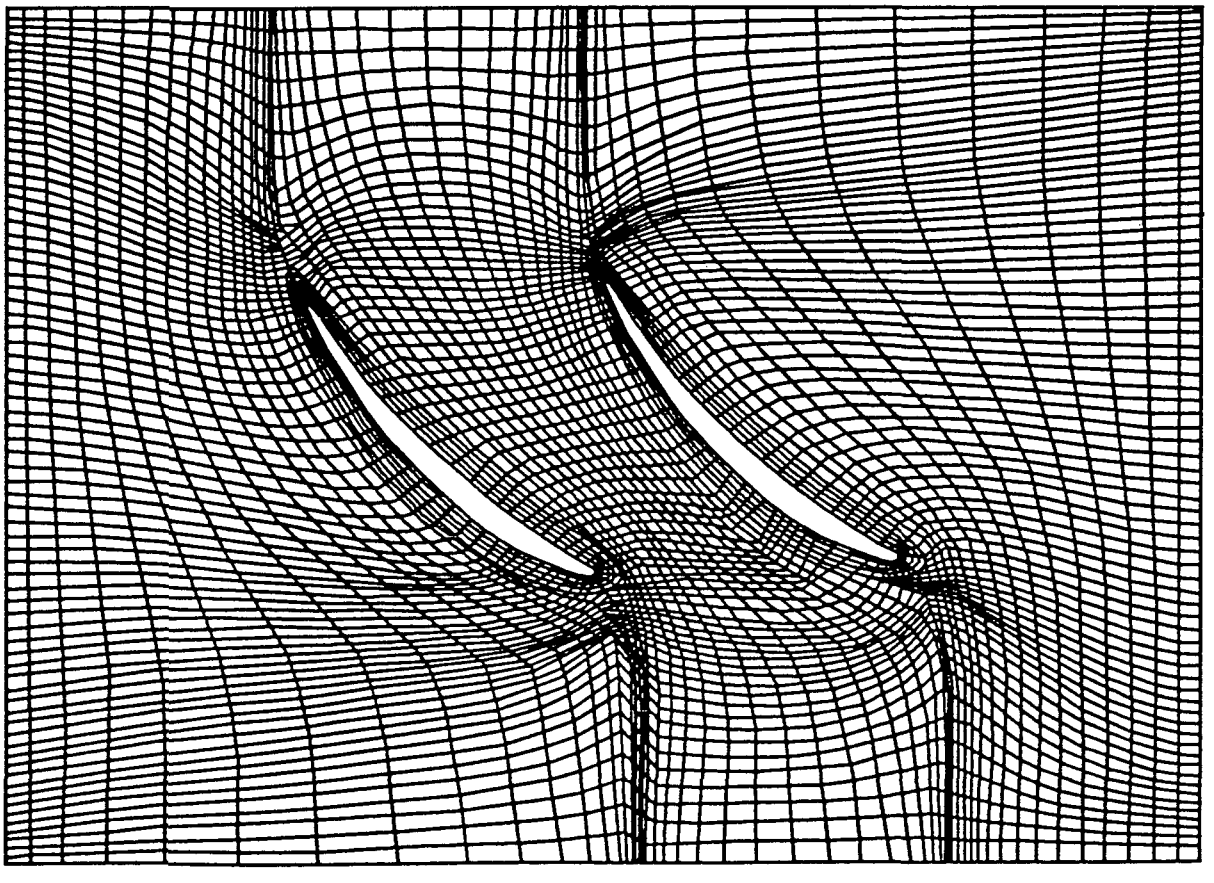

ORIGINAL

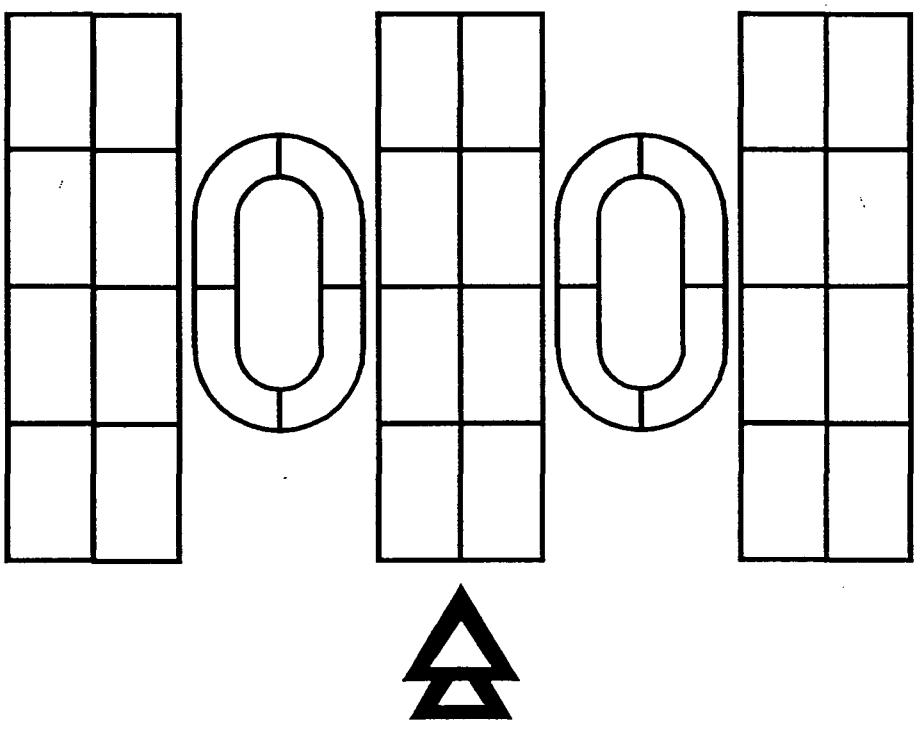

TOPOLOGICAL EQUIVALENT

Figure 2

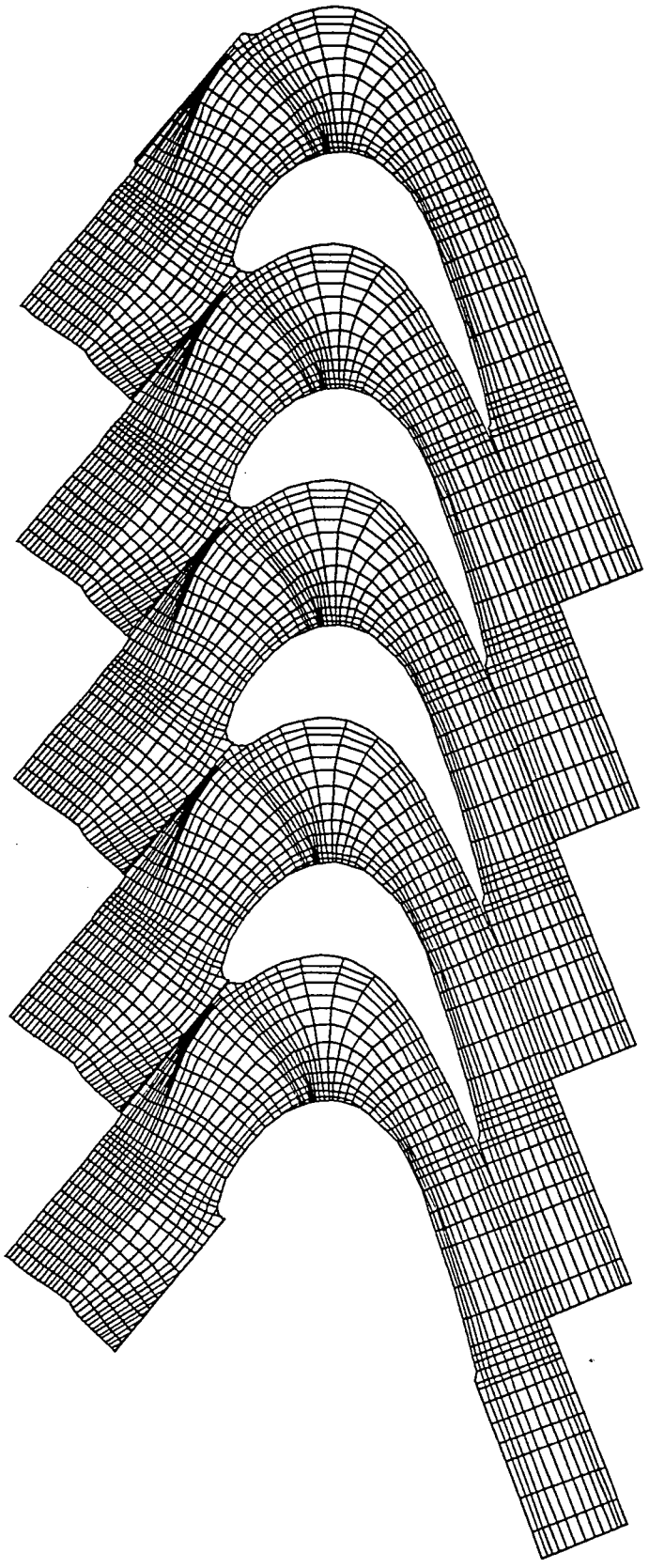

Figure 3

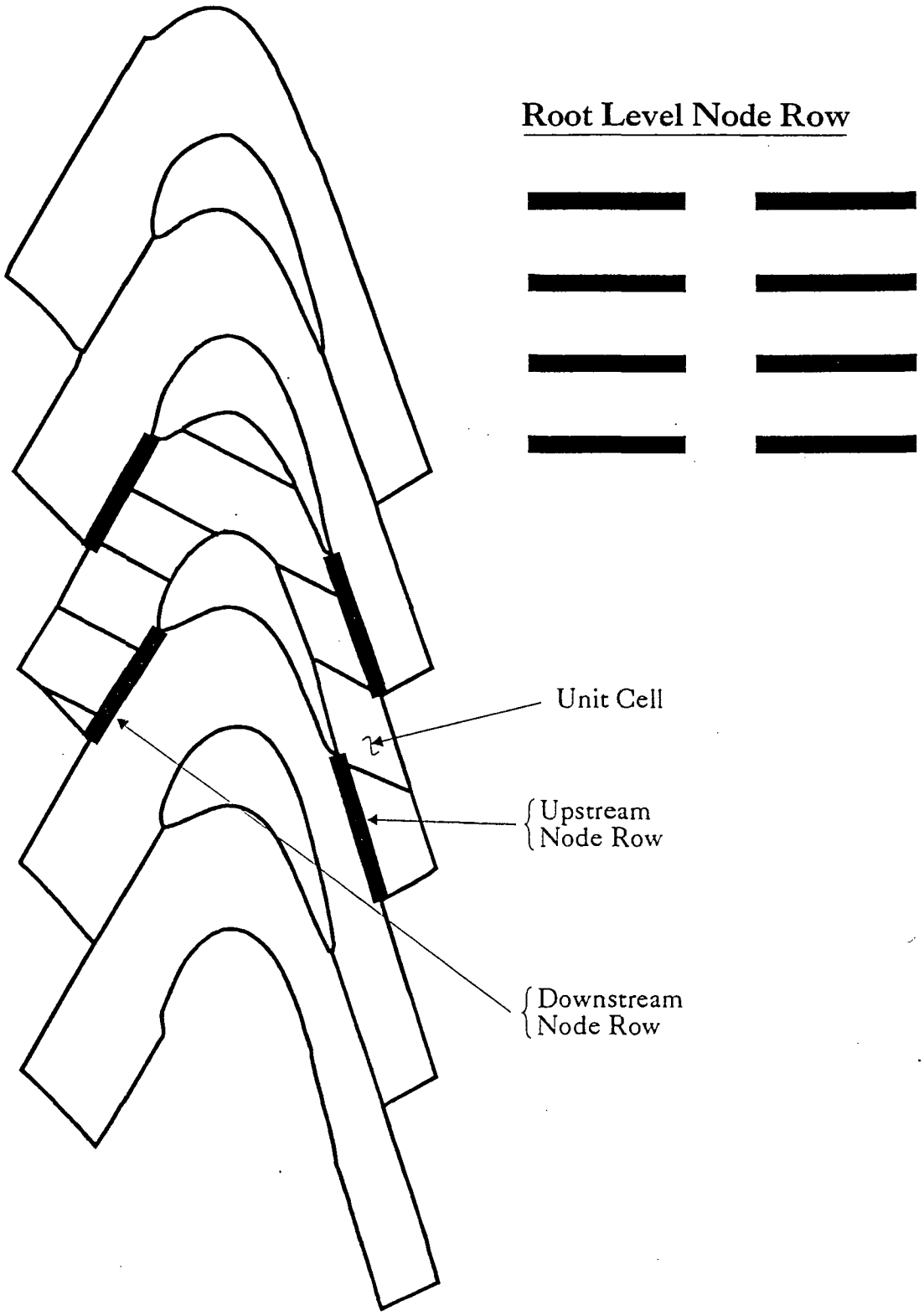
Root Level Node Row
Unit Cell
Upstream
Node Row
Downstream
Node Row

Figure 4

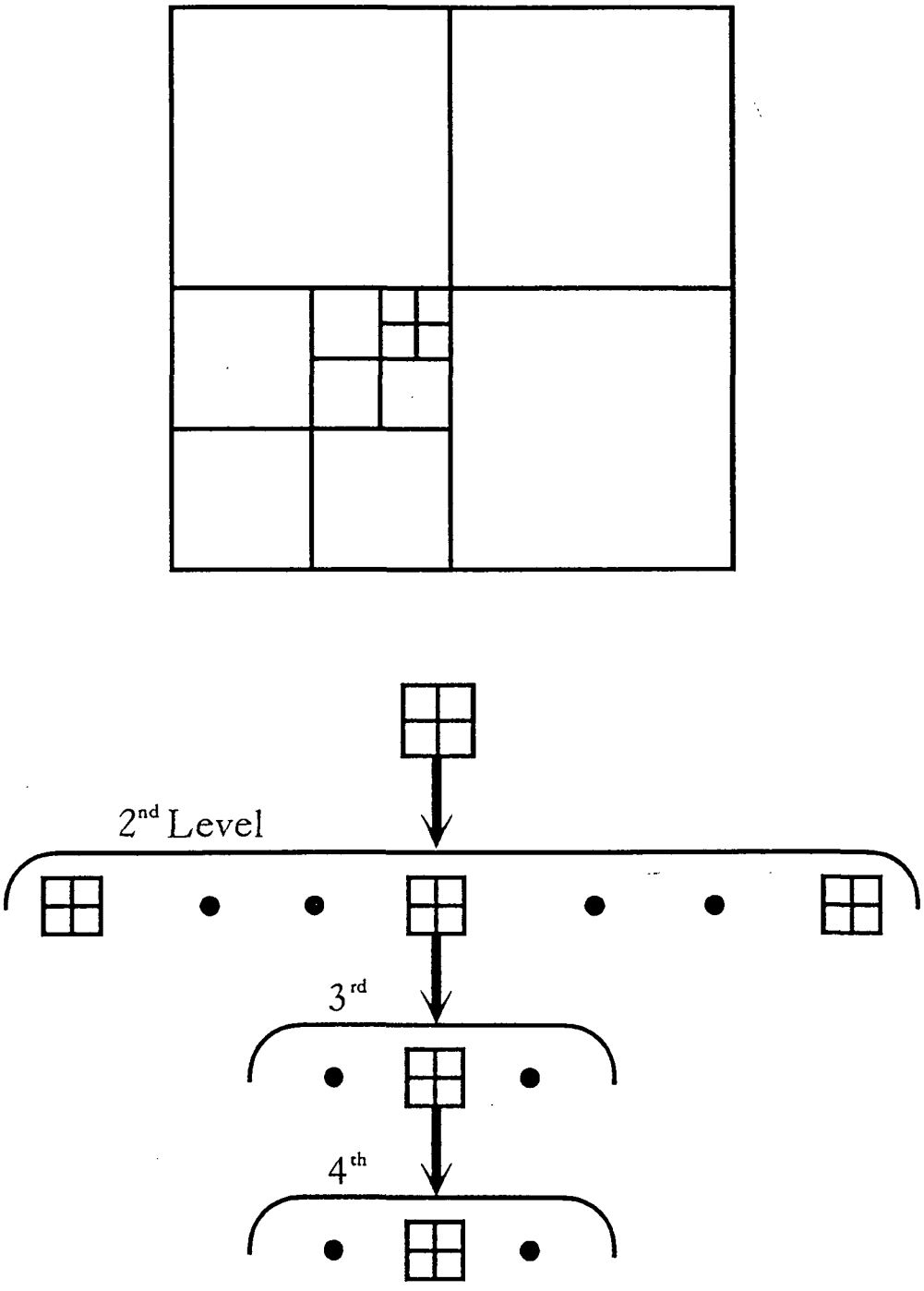

Figure 5

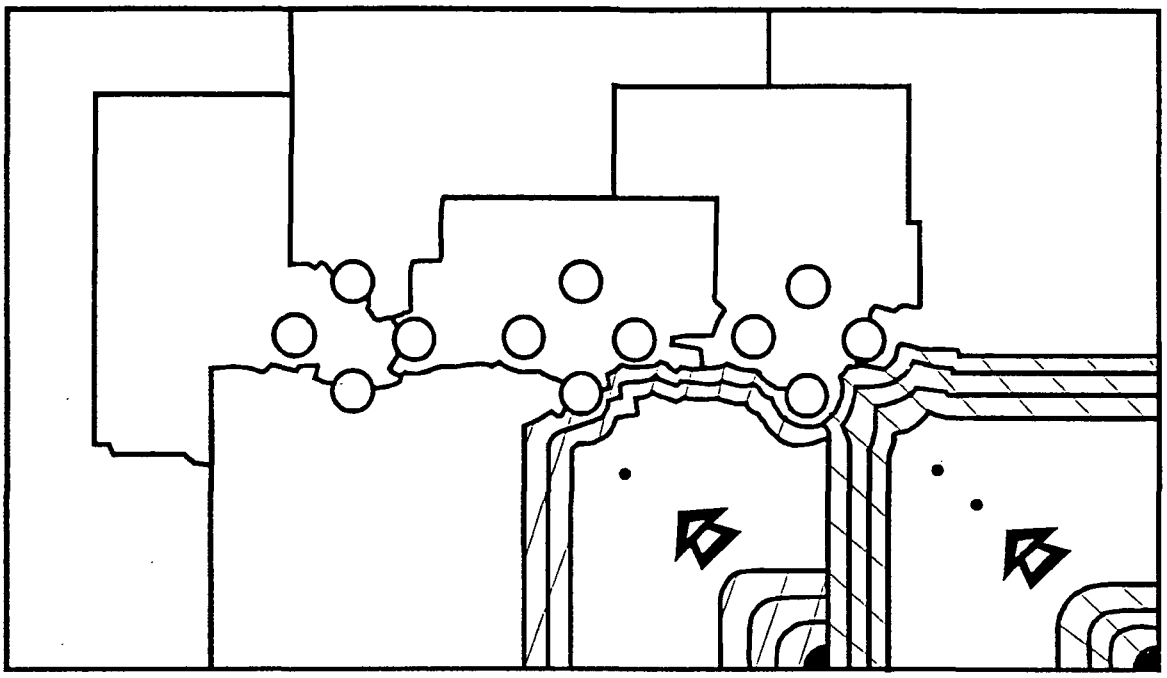

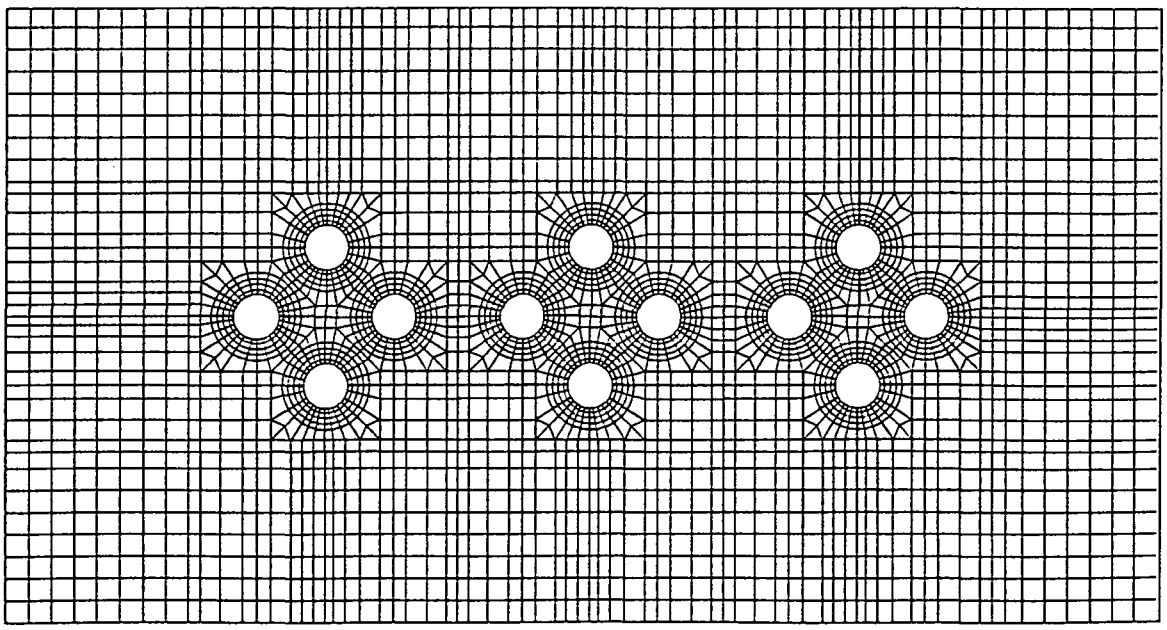

Figure 6

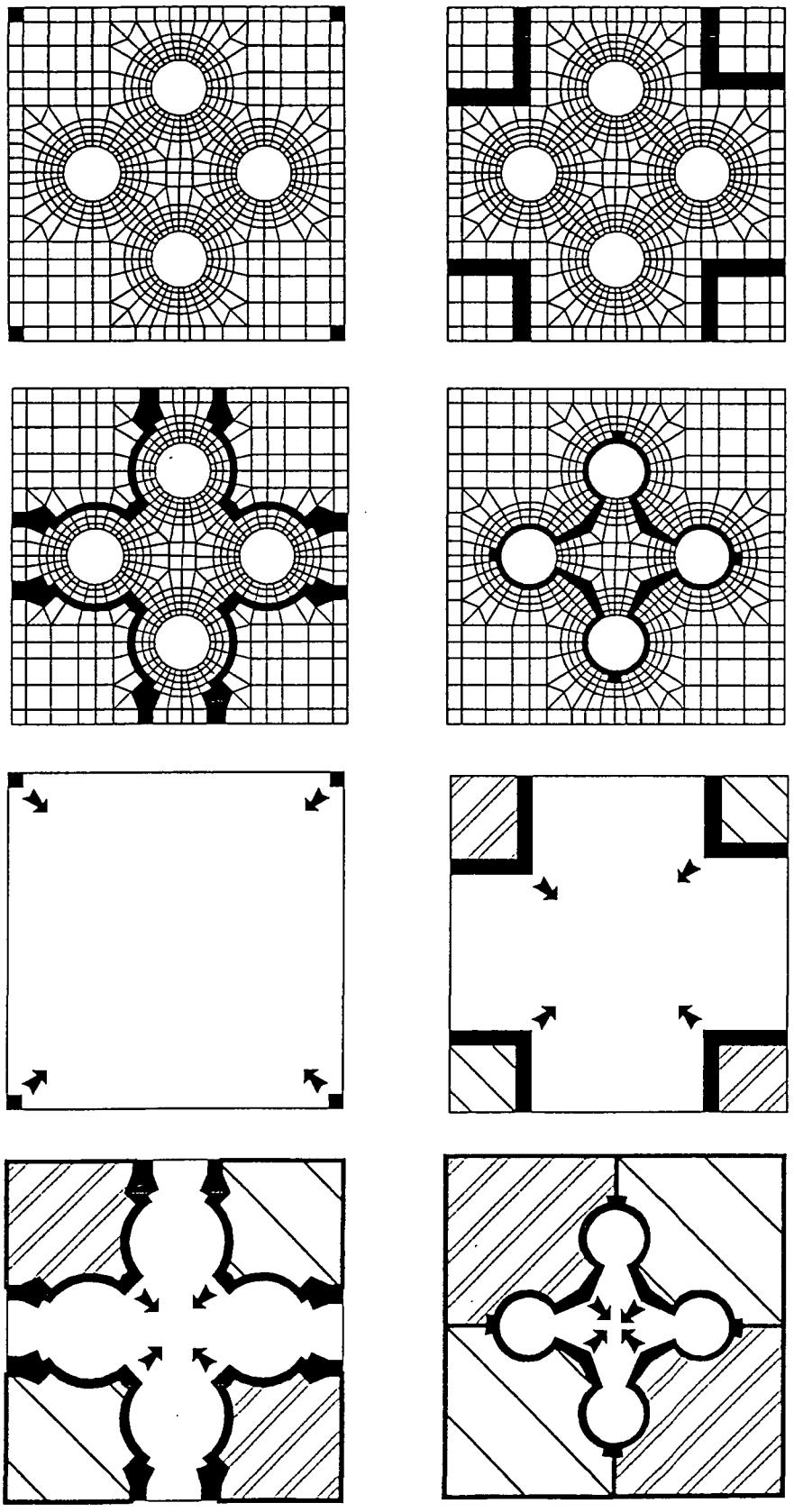

Figure 7

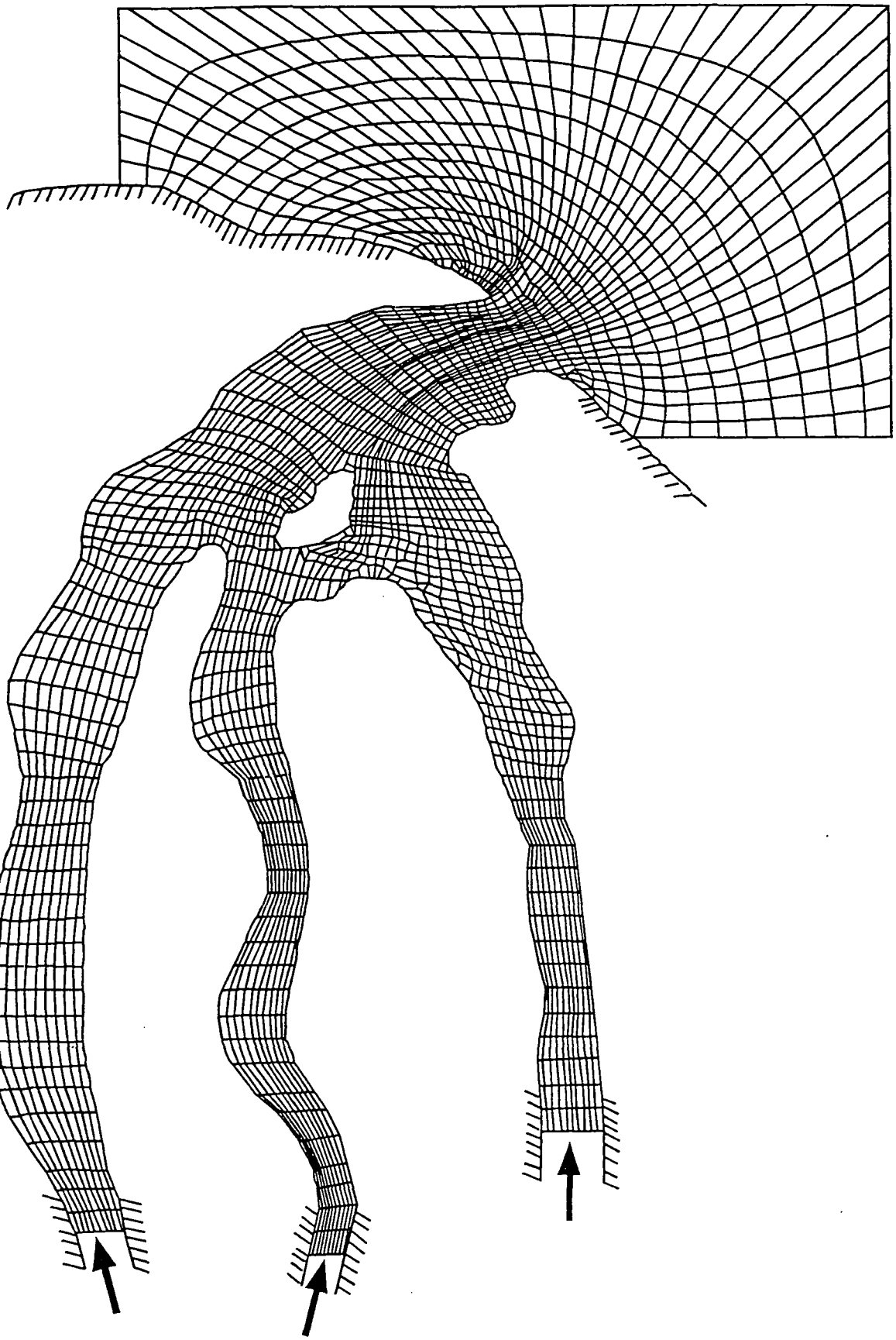

Figure 8

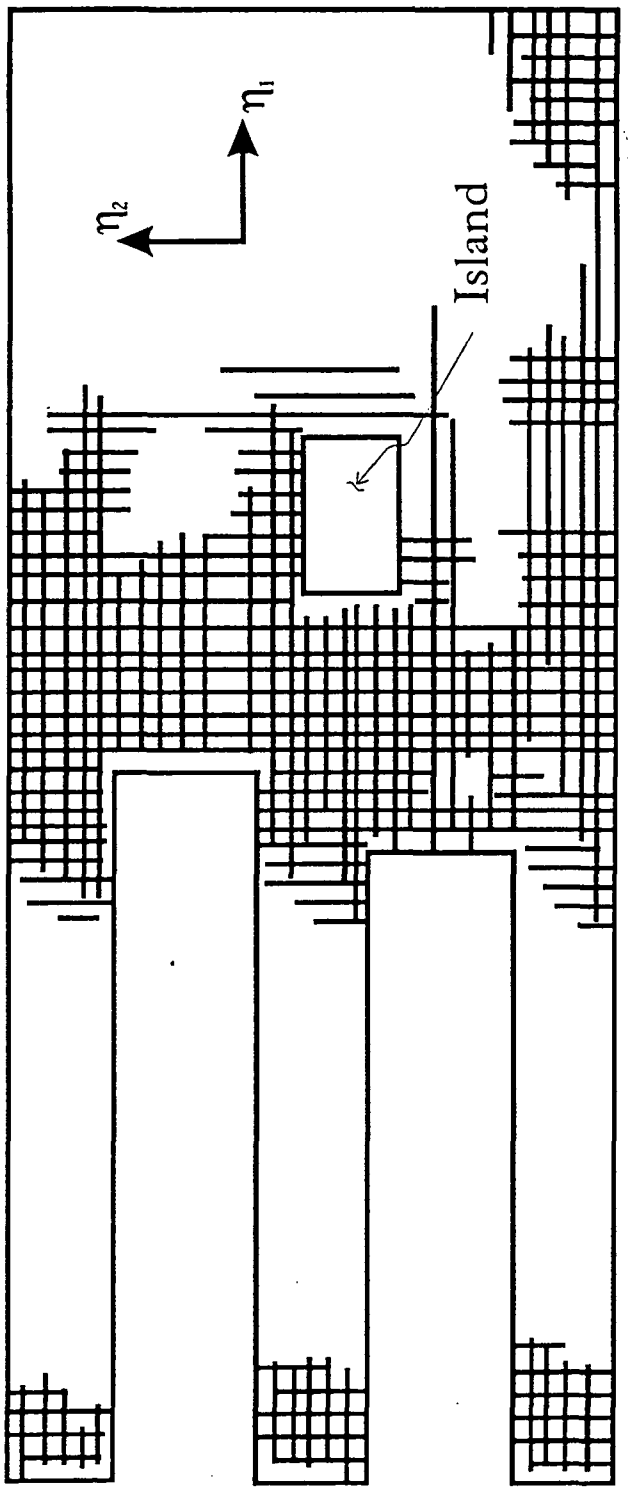

Figure 9

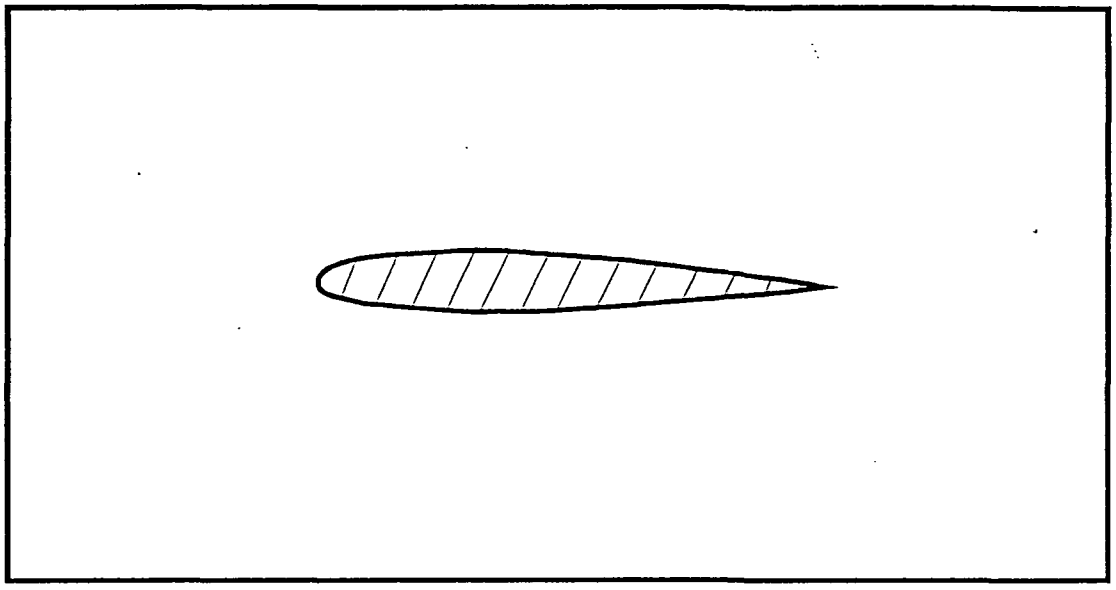

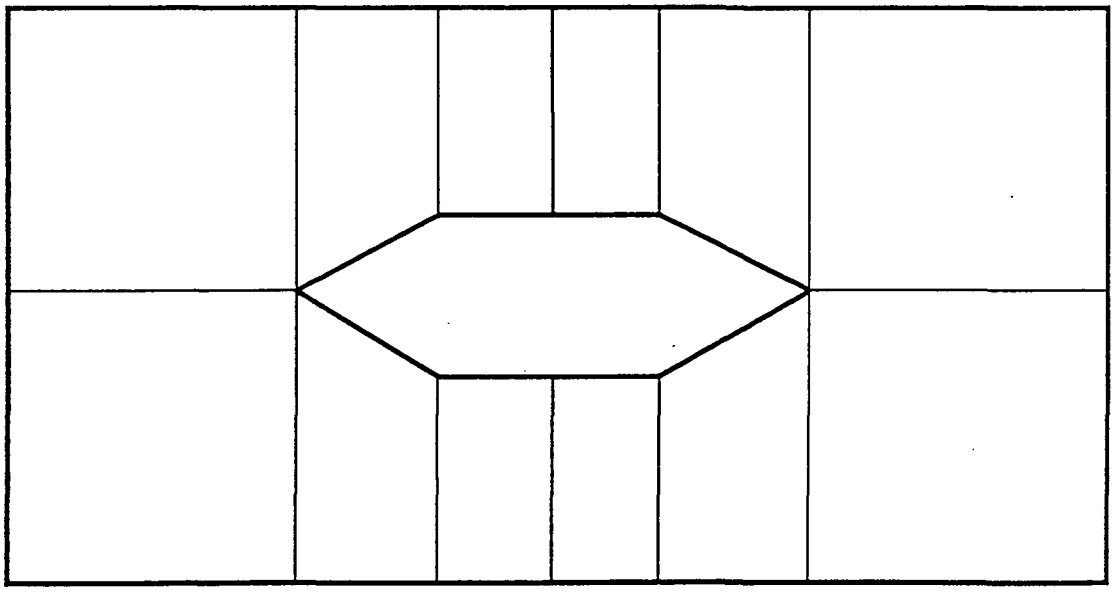

Figure 10

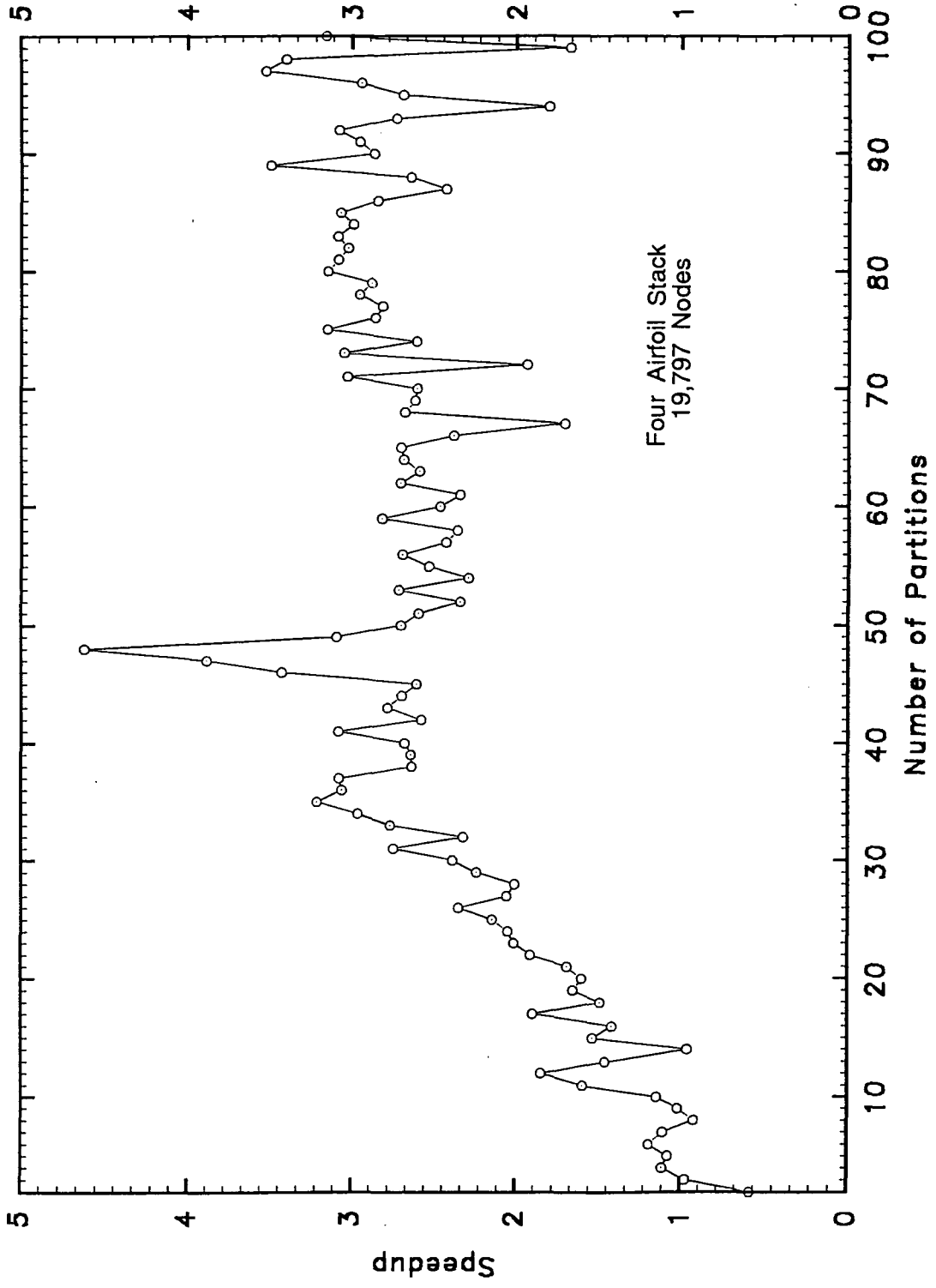

Figure 11

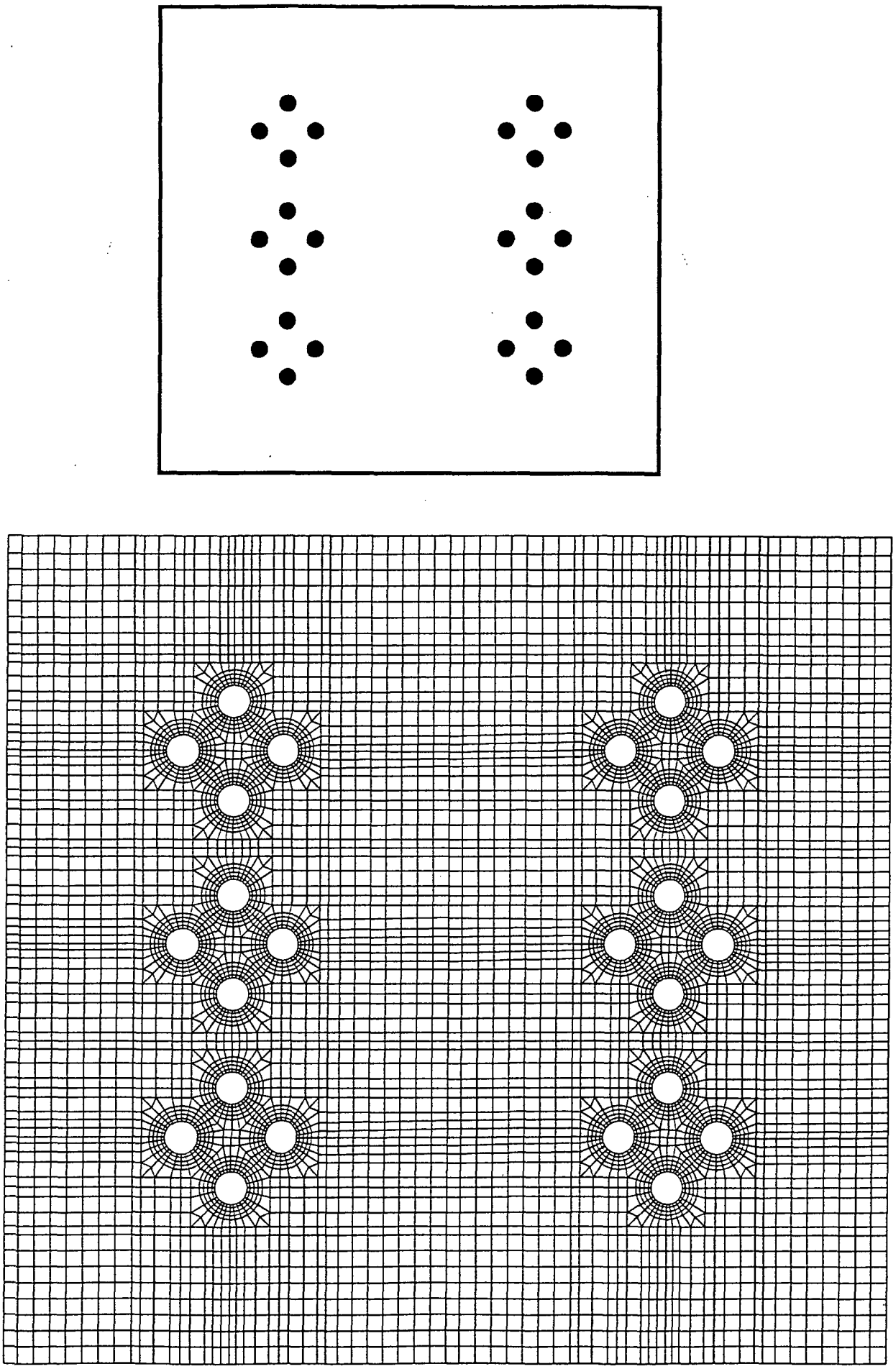

Figure 12

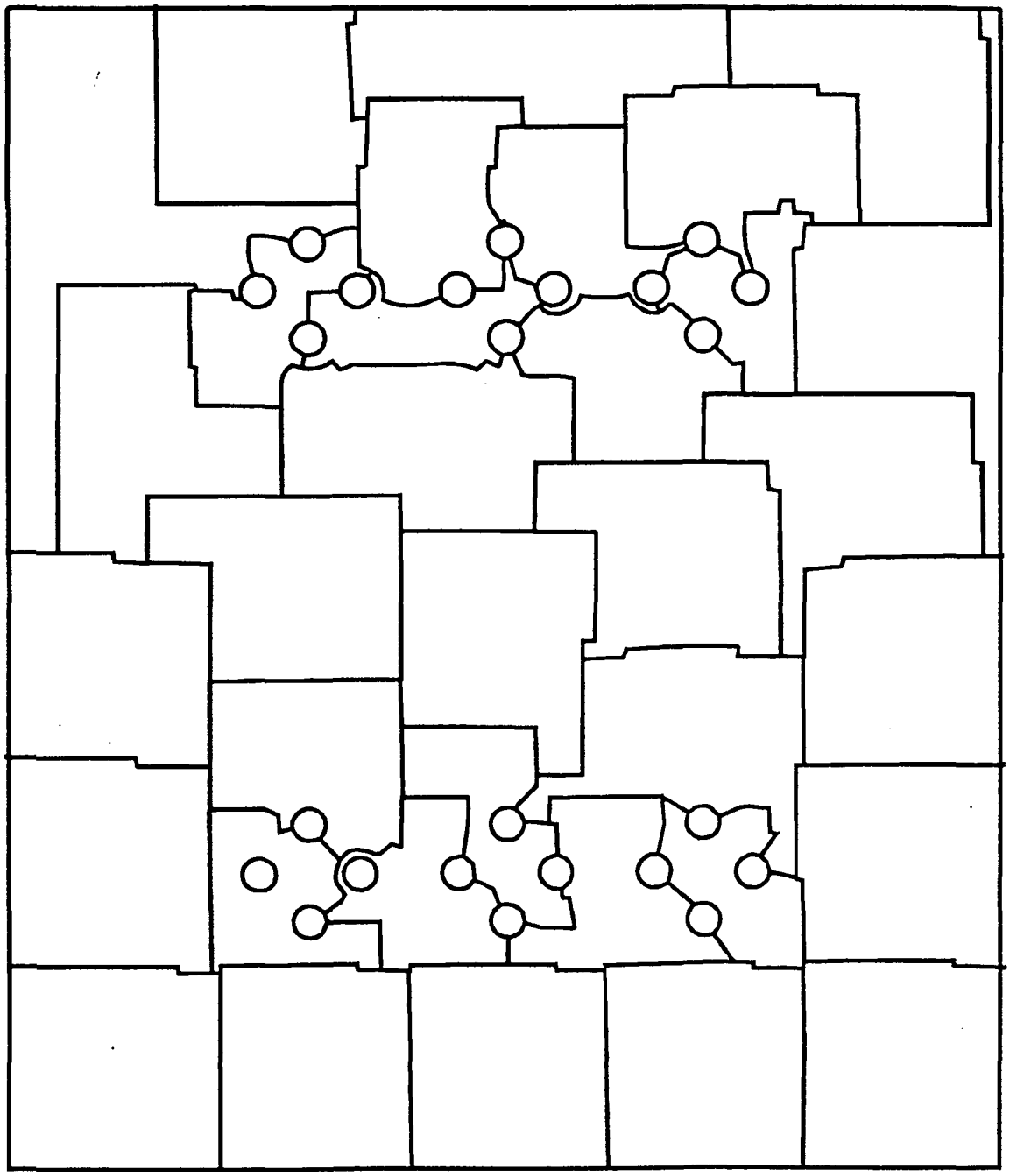

Figure 13

Table Captions

Table 1 Charleston Harbor Model: Sequential Speedup

Table 2 Four Turbine Blade Model: Sequential Speedup

Table 1

Model/ Nodes	Two Level Tree		Three Level Tree	
	Effort Speedup	Memory Reduction	Effort Speedup	Memory Reduction
small 2207	1.80	1.30	2.95	1.43
medium 8036	2.51	1.60	4.25	1.93
large 18081	2.50	1.72	5.31	2.37

Table 2

Three Level Tree, nodes = 19718			
Partitions/Levels 2	3	Effort Speedup	Memory Reduction
12	25	11.53	3.42
12	64	12.50	3.56
48	25	12.97	3.75
48	100	13.13	3.60

Four Level Tree				
Partitions/Levels 2	3	4	Effort Speedup	Memory Reduction
3	25	64	13.16	3.61
4	12	25	9.44	3.20
12	16	25	17.59	3.85
12	20	20	10.23	3.17